A fundamental study of injection and combustion characteristics of neat Hydrotreated Vegetable Oil (HVO) as a fuel for light-duty diesel engines

Fuel 379 (2025) 132951

Contents lists available at ScienceDirect

Fuel

journal homepage: www.elsevier.com/locate/fuel

Full Length Article

A fundamental study of injection and combustion characteristics of neat Hydrotreated Vegetable Oil (HVO) as a fuel for light-duty diesel engines

Federico Millo [a,*], Mohammad Javad Jafari [a], Andrea Piano [a], Lucio Postrioti [b], Gabriele Brizi [c], Alberto Vassallo [d], Francesco Pesce [d], Corrado Fittavolini [e]

[a] Politecnico di Torino, Energy Department, Italy
[b] Università degli Studi di Perugia, Italy
[c] Shot-to-Shot Engineering S.r.l., Italy
[d] Dumarey Automotive Italia S.p.A., Italy
[e] Eni S.p.A., Italy

ARTICLE INFO

Keywords:
Hydrotreated Vegetable Oil
Fuel spray characteristics
LD diesel engine
Combustion
CO_2 emissions
Pollutant emissions

ABSTRACT

Renewable fuels are essential for decarbonization because they can significantly reduce greenhouse gas emissions compared to fossil fuels. Among the renewable fuels capable to be mass produced, Hydrotreated Vegetable Oil (HVO) is attracting major attention thanks to its noticeable physical and chemical properties, which make it a viable and effective diesel substitute.

In this work, the fundamental injection and combustion characteristics of neat Hydrotreated Vegetable Oil (HVO) as an alternative fuel for light-duty diesel engines have been analysed by means of an extensive experimental campaign based on a single injection strategy in both spray and engine laboratory tests.

A Euro 6 light-duty diesel engine was selected as a case study for the research activity, comparing the neat HVO injection, combustion, and emission characteristics with those of a B5 diesel fuel. Differences were firstly scrutinized in terms of injection rate and main spray characteristics, these latter by means of both spray imaging and Phase Doppler Anemometry (PDA) techniques. Then, engine tests were performed for three different operating conditions (at low, medium, and medium–high load, respectively) to investigate the combustion properties and emissions. Furthermore, the sensitivity of neat HVO and B5 diesel to different Exhaust Gas Recirculation (EGR), Start of Injection (SOI), and injection pressure levels was also explored. In conclusion, HVO showed an excellent adaptability to nowadays automotive diesel engines also as a neat fuel without the necessity of a specific engine recalibration, allowing to achieve an impressive 85% reduction in terms of CO_2 emissions on a WTW basis, with a limited increase (lower than 4%) in volumetric fuel consumption and with impressive reductions in terms of CO and HC emissions (more than 40 and 50 %, respectively).

1. Introduction

In light of the urgent need to address climate change, governments worldwide are setting ambitious goals to cut down greenhouse gas (GHG) emissions. The European Union in particular aims to achieve carbon neutrality by 2050 in the transportation sector [1] which contributes about one-fifth of the global CO_2 emissions [2].

However, while the commonly accepted belief promotes the electrification of road transportation as the ultimate solution, rapidly shifting all modes of transport to electric propulsion might not be possible and may not be the most effective approach for reducing carbon emissions in on-road transportation.

A recent study by FFV, Germany-based worldwide innovation network [3], provided a comprehensive analysis of different powertrain technologies for the European transport sector, concluding that "the speed of deploying GHG-neutral mobility solutions… is much more important than the choice of technologies. … The majority of GHG emissions are caused by the phase-out of the vehicle fleet, which is still operated with fossil energy carriers. Therefore, the faster a defossilized vehicle fleet can be introduced, the lower are the cumulative GHG emissions and the impact on climate change…The ramp-up speed of fully sustainable technology pathways is the decisive factor for minimizing the global warming impact of the transport sector, and a mix of

* Corresponding author.
E-mail address: federico.millo@polito.it (F. Millo).

https://doi.org/10.1016/j.fuel.2024.132951
Received 25 April 2024; Received in revised form 19 August 2024; Accepted 27 August 2024
Available online 4 September 2024

Nomenclature

Acronyms

aTDC	after Top Dead Center
BMEP	Brake Mean Effective Pressure
BSCO	Brake Specific Carbon Oxide
$BSCO_2$	Brake Specific Carbon dioxide
BSFC	Brake Specific Fuel Consumption
BSNOx	Brake Specific NOx
BSSOOT	Brake Specific Soot
BTE	Brake Thermal Efficiency
CA	degree of Crank Angle
CAC	Charge Air Cooler
CN	Cetane Number
CoV	Coefficient of Variation
CVC	Constant Volume Chamber
EGR	Exhaust Gas Recirculation
ET	Energizing Time
ECU	Engine Control Unit
FAME	Fatty Acid Methyl Esters
FSN	Filter Smoke Number
GHG	Green House Gases
GDI	Gasoline direct Injection
GTL	Gas-To-Liquid Diesel
HC	Hydrocarbons
HD	Heavy-duty
HP	High Pressure
HRR	Heat Release Rate
HVO	Hydrotreated Vegetable Oil
Ig. D	Ignition Delay
ICE	Internal Combustion Engine
LCA	Life Cycle Assessment
LD	Light Duty
LHV	Lower Heating Value
LP	Low Pressure
MFB10	10 % Mass Fraction Burned
MFB50	50 % Mass Fraction Burned
NOx	Nitrogen Oxides (NO, NO2)
OME	Oxymethlyenether
PAH	Polycyclic Aromatic Hydrocarbons
PDA	Phase Doppler Anemometry
P_{inj}	Injection Pressure
PL	Penetration Length
PM	Particulate Matters
PRR	Pressure Rise Rate
PVC	Pressure Control Valve
rpm	Engine speed as revolution per minutes
SOI	Start Of Injection
SMD	Sauter Mean Diameter
TDC	Top Dead Center
vol.	volumetric
VGT	Variable Geometry Turbocharger
WTT	Well-To-Tank
WTW	Well-To-Wheel

carbon–neutral pathways (energy forms and powertrains) can speed up the transition to GHG neutrality significantly compared to single-technology scenarios.”.

These findings stress the importance of adopting a diversified approach to powertrain technology, including solutions like bio and e-fuels for internal combustion engines to speed up progress towards sustainable and carbon–neutral transportation systems.

Among renewable fuels Hydrotreated Vegetable Oil (HVO) is recognized as one of the most promising, with its production and use rapidly increasing worldwide. The potentiality of using waste materials (such as non-edible vegetable oils, agricultural residues, animal wastes, etc.) as its feedstock, as well as the possibility of using the existing infrastructure, make HVO a feasible option to contribute to achieve our decarbonization goals. HVO is a second-generation biofuel as it is a product of hydrotreatment of triglycerides derived from non-edible vegetable oils, animal fats, and discarded cooking oils [4]. Being produced from renewable sources, HVO can provide significant reductions in terms of CO_2 emissions in comparison with conventional diesel fuel from fossil sources from a Well-To-Wheels (WTW) perspective: Schwarz et al. [5] for instance reported an overall CO_2 reduction of up to 85 % in comparison with fossil fuels. Moreover, according to a WTT analysis carried out by ENI [6], HVO emits about 17.6 g/MJ equivalent CO_2 which is about 81 % lower than the equivalent CO_2 emitted by the reference fossil mix defined by RED II (2018/2001/EU), which is estimated to be 94 gCO2eq/ MJ (Fig. 1). In addition to these benefits in terms of GreenHouse Gasses (GHG) emissions reduction, the physio-chemical characteristics of HVO, and in particular its paraffinic structure as a long-chain alkane with saturated bonds, and the lack of aromatics and sulphur, result in lower pollutant emissions [5].

Despite the impact of HVO on fuel injection, combustion and pollutant formation processes in internal combustion engines has been widely investigated in recent years ([7,8]), the results reported in literature are not always in agreement, and in some cases even contradictories. This can be ascribed not only to the variabilities in the fuel properties depending on the feedstock and on the production process, but also to the different applications and test conditions (e.g. heavy or light duty engines, tests with or without specific engine re-calibration, etc.).

Therefore, the aim of the current research activity is to understand the root causes of the abovementioned discrepancies, focusing on a Euro 6 light-duty vehicle application.

The methodology is to adopt an extended experimental campaign

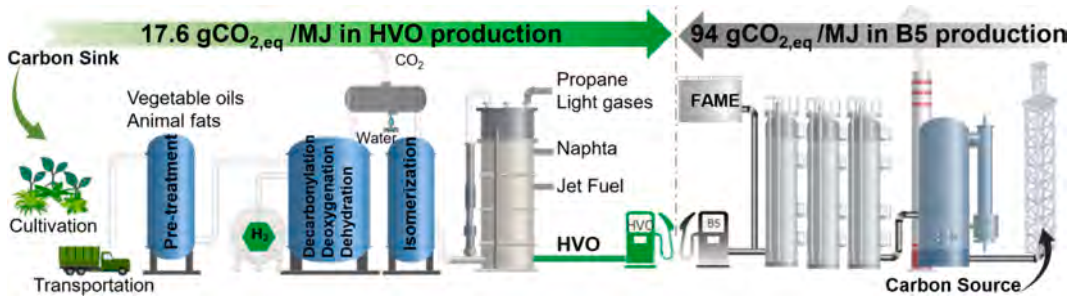

Fig. 1. Schematic view of HVO production vs. commercial diesel.

that encompasses injection hydraulic and spray imaging and sizing tests with initial and boundary conditions that closely resemble the fuel injection processes within a light-duty diesel engine, and then engine tests in different operating conditions. The major feature of the adopted methodology is the adoption of a single injection strategy in all the injection and combustion tests so to fully understand the impact of HVO characteristics on injection and combustion processes, as well as on the interactions between the two, eliminating the effects of pilot and post injections as well as the impact of engine calibration. This approach represents a fundamental and first phase of a wider research project, aiming to explore and analyse the effects of HVO chemical and physical properties on its behaviour as a fuel in Euro 6 and post Euro 6 passenger car diesel engines, so to pave the way for a complete replacement of fossil diesel with HVO and other renewable fuels.

In this framework, this paper is structured as follows: firstly, a literature review is presented. Then, details about the experimental setup, encompassing fuel injection, spray analysis, engine tests, and fuel characteristics are provided. Finally, the results coming from the injection and the engine tests are discussed, and conclusions about the impact of HVO properties on injection, combustion and emissions formation processes in a Euro 6 LD engine are drawn.

2. Literature review

In this Section, the results of the most relevant studies concerning HVO injection and combustion characteristics will be discussed.

As far as the impact of HVO on the fuel spray is concerned, quite modest or even negligible differences in spray characteristics of HVO and diesel were reported in [9], where Cheng et al. showed that the differences of HVO and Diesel in terms of spray penetration, angle and volume at low ambient air density conditions were about − 2 %, 13 %, and − 13.3 % respectively, with even lower differences at high ambient air density conditions. Modest variations with respect to diesel of some HVO spray features such as a slightly lower tip penetration due to its lower density were also reported in other works, such as for instance in [10] and in [11], while the spray cone angle of both fuels was generally found to be similar.

On the contrary, Bohl et al. [12] reported wider cone angles for HVO. The different results reported in the literature for HVO, and diesel cone angles likely root back to the fact that the cone angle is mostly affected by two factors: break-up and evaporation, with a more intense break-up leading to wider cone angle, as well as a faster evaporation. Therefore, both fuel viscosity and ambient temperature conditions during the tests are playing a major role. However, kinematic viscosity values at 40° C for HVO reported in literature may range from 2.6 to 3.8 mm^2/s, depending on the feedstock and on the production process. Also, the experiments have been carried out at different ambient temperatures, thus leading to even opposite results in some cases.

Conversely there is a general agreement about the spray tip penetration of HVO, that is always slightly lower than that of diesel, since the penetration length is less influenced by the ambient conditions while it is more predominantly determined by the spray momentum, and therefore by the fuel density. However, yet some contradictory reports can be found in the literature. An example is Ref. [13] in which the measured HVO liquid penetration length was reported to be slightly higher than that of diesel at 120 and 180 MPa injection pressure and room temperature. In this case the HVO longer penetration length was attributed to its higher mass flow rate as a consequence of its lower viscosity.

Dageförde et al. [14] measured the velocity field in the primary atomization region of HVO, GTL and OME and found that the nozzle outlet velocity of HVO droplets is about 20 % higher than OME droplets but the deceleration rate of the HVO droplets as the spray propagates downstream is higher due to higher Weber number, which can be a sign of a more intense air–fuel interaction. Although their report does not include standard diesel, it can be expected diesel droplets showing intermediate values between those of HVO and OME for acceleration and deceleration parameters for the same reason. Therefore, also in the area of fuel spray macroscopic and microscopic characteristics a more comprehensive and in-depth analysis appears to be necessary.

Finally, as far as HVO combustion in ICEs is concerned, the wide literature background has to be divided into two main categories on the basis of the application, since the combustion processes in light duty and heavy-duty engines can be significantly different, and the same is for the impact of the HVO. Since the focus here is on LD applications, reports about HVO in HD vehicles and marine applications (such as [15–17]) which are here reported for completeness, will not be discussed hereafter. For a EURO 6 light-duty engine Omari et al. [18], reported that PM, HC, and CO emissions were reduced when HVO was used in in two different drop-in scenarios, one with a constant injection timing and the other with a constant combustion phasing, i.e., with a constant 50 % Mass Fraction Burned (MFB50) angular position. However, they reported an increase in NOx emissions for both drop-in scenarios. Mixed trends for NOx were instead reported by other researchers such as Dimitriadis et al. [19], while Bhardwaj et al. [20] with constant MFB50, measured almost constant NOx emissions, while measuring lower values for all other pollutants with HVO under low, medium, and full load operating conditions.

Along with positive effects on all other criteria pollutants, Di Blasio et al. in [21] observed non unique effects of HVO on Particle Number (PN) when comparing diesel and neat HVO in an advanced Euro 6 Single-Cylinder Engine (SCE) and implementing complex multi-pulse injection patterns. Similar results on an SCE were also found by Bortel et al. [22] for different steady-state operating points tests. They claimed these not conclusive findings about PN emissions could be attributed to the effects of the dwell time between pilot and main injections, suggesting the need for additional analysis of the combustion process to be carried out, as the present work aims to do. To this aim, Sugiyama et al. [23] considered both single injection and pilot-main injection schedules at different engine loads and found remarkable differences in HVO combustion and emission records for the two schedules. In particular, they found that HVO effects on ignition delay, heat release rate and smoke emissions are always more evident and more pronounced when the pilot injections are omitted.

Furthermore, Hunicz et al. [24] included single injection strategy tests in their experimental matrix on a single-cylinder engine, aiming to explore the HVO potential to support the attainment of Partially Premixed Compression Ignition (PCCI) in a contemporary engine platform.

In conclusion, even if several examples have been reported in literature concerning the analysis of the impact of HVO characteristics on the combustion process in case of single injection strategies, a comprehensive analysis of the effects on both fuel injection and spray and combustion on the same engine has not yet been carried out. This research aims to cover this gap since it is of paramount importance to highlight the HVO impact on the interactions between the injection and the combustion processes. Understanding the effects of HVO's physical and chemical properties (which can be significantly different with respect to those of diesel fuel) on both injection and combustion processes is indeed of paramount importance to fully exploit the potential of HVO as a diesel substitute in LD engines, paving the way to the next steps of the current research program, which will focus first on the HVO exploitation as a "drop-in" diesel substitute, and then on possible further benefits coming from engine specific recalibration.

3. Experimental set-up

3.1. Test fuels

The experimental tests have been carried out comparing a "standard" EN590 diesel (hereafter referred to as B5, due to its 5 % content of biofuel as Fatty Acid Methyl Ester, FAME) as the reference fuel and neat Hydrotreated Vegetable Oil (HVO). The main properties of the test fuels

Table 1
Main properties for B5 diesel reference fuel and HVO used in this study.

Properties Unit		B5	HVO
Cetane Number	–	54.6	79.6
Density (@15 °C)	kg/m3	830.6	777.8
LHV	(MJ/kg)	42.65	44.35
Viscosity at 40 °C	mm^2/s	2.97	2.65
Carbon	% m/m	86.2	85
Hydrogen	% m/m	13.8	15
FAME	% v/v	5	0.05
Sulphur	mg/kg	6.5	0.53
Water	% m/m	0.010	0.004
Total aromatics	% v/v	23	0
Inflammability	°C	74	60.5
Boiling point (T95)	°C	351	296
Cloud point	°C	−5.00	−3.80
Cold Filter Plugging Point	°C	−6.0	−8.0

used in this study are listed in Table 1. The noticeable differences in HVO properties compared to B5 are the lower values of density and viscosity for HVO due to its molecular structure, the higher cetane number due to the long-chained acyclic, unbranched, and saturated C–H bonds in its molecule, and the higher Lower Heating Value (LHV) for HVO due to its higher hydrogen content and lack of oxygen [5].

3.2. Fuel injection system tests

In the first part of the present research activity, the fuel behaviour was investigated both in terms of hydraulic (i.e., injected quantity and injection rate) and of spray (e.g., penetration, atomization) characteristics at the SprayLab of the University of Perugia.

Hydraulic analysis

The actual hydraulic operation of the injection system when fed with neat HVO and B5 fuel was investigated in several operating conditions using a hydraulic test bench based on a complete “wet system”, i.e., an apparatus featuring the same components installed on the corresponding automotive injection system. The hydraulic bench layout is depicted in Fig. 2.

In the bench, a low-pressure pump delivers the fuel to the high-pressure pump (Denso HP3), driven by a 10 kW DC motor at 1000 rpm for the present campaign. The pressurized fuel is fed to the 4-cylinder common rail; the rail pressure is controlled in a closed-loop

Table 2
Phase Doppler Anemometry system characteristics.

Transmitter	112 mm
Receiver	HiDense 112 mm, screen A
Laser source	FlowLite 1D (532 nm, 200 mW)
Processor	BSA P80
Frequency shift	40 MHz
Focal length (TX/RX)	310 mm / 310 mm
Scattering Angle	110°
Ref. system origin (X=0; Y=0; Z=0 – Z downward)	Nozzle tip center

actuating the PCV metering valve at the high-pressure pump inlet. The 4 common rail injectors (Denso G3S) are operated according to the actual engine timing, using a programmable driver (NI-Driven 9751) to reproduce the prescribed solenoid current profile. With this arrangement the rail pressure time-history is very close to the engine-one, obtaining a fully realistic operation for the injection system. While the fuel injected by 3 of the 4 injectors is simply collected and returned to the fuel tank, the 4th injector is used for both the hydraulic and the spray analyses. The hydraulic analysis is based on a proprietary Injection Rate Analyzer (Inj. rate meter in Fig. 2) based on the Zeuch Method ([25,26,27]). This instrument performs a shot-resolved measurement of both the injection rate profile and of the injected quantity, in each assigned operating condition in terms of rail pressure and injector actuation strategy. During each injector actuation, fuel is injected in a constant volume measuring chamber, pressurized with the same fluid at a base level (40 bar in the present analysis) before the injection event.

The injected fuel causes the measuring chamber pressure to rise until it attains a higher steady level at the injector closure or – for a multi-event strategy – at the end of the final injection event. The fluid volume globally injected is proportional to the chamber pressure increase, while the injection rate is proportional to the time-derivative of the measuring chamber pressure during the event; for both these quantities, the ratio of the chamber volume to the fluid bulk modulus is the proportionality factor. The chamber pressure is detected by a piezo-resistive sensor Kistler 4075A100 and acquired at 100 kS/s, allowing the evaluation of both the injected quantity and injection rate on a shot-to-shot basis. After the completion of the injection pulse train, a fast-acting discharge valve is operated, re-settling the base pressure level in measuring chamber for the next measurement cycle. Since the bulk modulus of a given fluid is influenced by both temperature and pressure, the injected fuel evacuated from the measuring chamber is metered by a

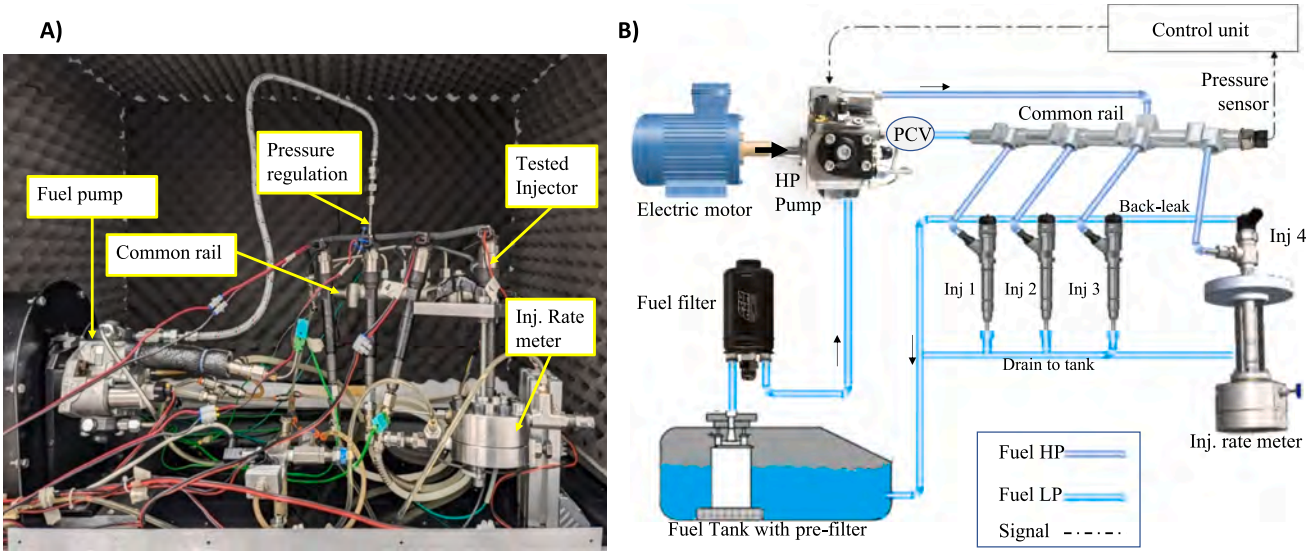

Fig. 2. Hydraulic test bench configuration (A) and its layout (B).

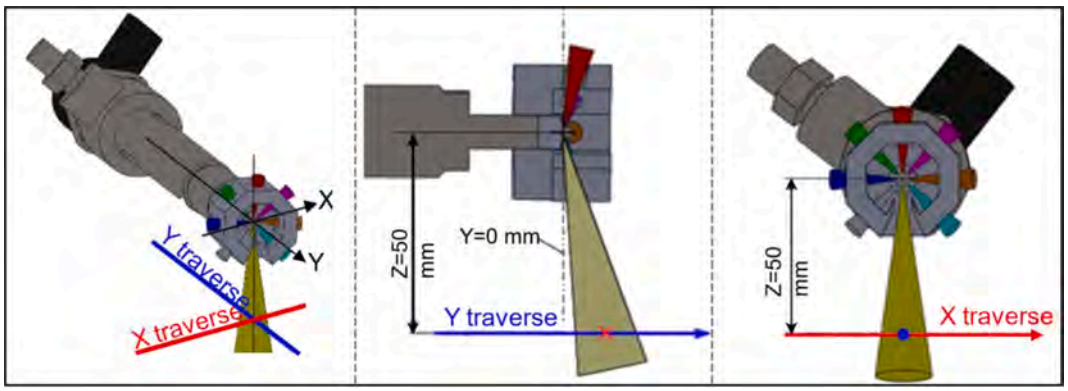

Fig. 3. PDA measurement set up.

Coriolis-type mass flow meter (Siemens Mass Flow 2100, ±0.1 % accuracy of the read quantity), performing a continuous calibration of the injection analyser in the actual operating conditions. Further details about the used Injection Analyzer are reported in [26] and [28].

The entire hydraulic test bench operation (DC motor control, rail pressure level control, injector-pump synchronization, injectors operation and data acquisition/analysis) is managed by a control system based on National Instruments cRIO hardware and software developed in LabVIEW environment.

Global spray analysis

The global spray evolution was investigated by imaging, so to describe the development of the single jets emerging from the nozzle; the jets evolution is quantitatively described by the obtained tip penetration, cone angle and bend angle (angular deviation of the jet cone bisector with respect to the nominal jet direction) curves per each single jet. This approach, despite being not as accurate in terms of actual targeting as a momentum flux spatial distribution analysis (e.g., [29]), is adequate to capture the fuel properties effects in terms of spray global shape. The imaging campaign was carried with the spray evolving in a Constant Volume Chamber (CVC), operated with air at ambient temperature at 20 bar, obtaining a 23.14 kg/m^3 density. Images were acquired frontally with respect to the nozzle axis, so to simultaneously visualize all the 8 jets. For the acquisition, an ensemble-average approach was followed, with one image per injection event acquired at a given delay from the synchronization trigger (the logic start of injector current); 30 images per timing were acquired in the present campaign, so to gain a statistically appropriate description of the spray shape dispersion at the considered timing. A pulsed Nd-Yag laser was used as lighting source, featuring a high energy per pulse (200 mJ) and an extremely short pulse duration (<10 ns), that significantly reduces the blur-effect in the acquired images. The laser light was guided through an annular fibre co-axial with the injector body, so to frontally illuminate the different jets emerging from the nozzle. A 2000x2000 pixel JAI Rm-4200 CMOS camera synchronized with the laser pulse emission was used for the image acquisition.

Spray atomization (Phase Doppler Anemometry)

The drop sizing and velocimetry analysis in high counter-pressure conditions was carried out in the same CVC used for the imaging analysis, using a 1-D Phase Doppler Anemometry (PDA) apparatus by Dantec Dynamics. The PDA system is based on a BSAP80 processor, a 112 mm Fibre PDA transmitter and a 112 mm Hi-Dense receiver, specifically designed to operate with dense spray such as Diesel or GDI jets; other details of the used PDA system are reported in Table 2. For the present analysis, the PDA transmitter and receiver probes faced two 100 mm-diameter quartz windows on the CVC, with a 110 deg angle among the probes (forward scattering arrangement).

In order to allow PDA measurements to be carried out in different positions inside the spray structure, the two probes were rigidly connected and positioned by a 3-axis Cartesian traverse system, according a XYZ refence system centred in the nozzle tip, with the Z-axis downward oriented. Using this approach, the spray drops sizing and velocity were measured along X and Y orthogonal traverses over the Z=50 mm plane Fig. 3). To limit the chamber fogging and improve the PDA measurement quality only one jet was investigated by PDA, with the fuel injected by the remaining 7 holes being intercepted by a specifically designed nozzle cap. The cap was 3D printed and featured 7 collecting pipes, with an appropriate air gap to the nozzle not to produce any fluid splash or bounce. For this fundamental analysis of HVO's different properties on the injection and spray characteristics, all the hydraulic and imaging tests were carried out using a single injection schedule which guarantees a clearer demonstration of the differences between HVO and B5 by eliminating the effects of pilot or post injections. The test cases' specifications are tabulated in Table 3.

Table 3
Specifications of the spray and injection tests cases.

Test name	Test equipment	Set up	P_{inj} (bar)	ET (μs)
Hydraulic	Injectors: Denso 55,570,012 Injector nozzles:8 Injector nozzles diameter: 0.12 mm Injector pump: Denso HP3	$T_{chamber}$: 25 °C $P_{chamber}$: 50 bar	500 100 1500	From 300 to 1200 From 240 to 1200 From 220 to 900
Imaging	CMOS Camera: Dantec Flowsense JAI Mono Lighting System: Litron Pulsed Nd-YAG 532 nm laser + 125 mm ringlight (front) Objective: Nikon 50 mm	$T_{chamber}$: 25 °C $P_{chamber}$: 20 bar	500 1500	400 and 800 250 and 800
PDA	Dantec Dynamic PDA System Fiber PDA Emitting Probe 38 mm with Beam Expander – Focal length 310 mm. HiDense Receiving Probe 112 mm – Focal length 310 mm – P80 Processor		500 100 1500	800 530 425

3.3. Engine and experimental setup

The engine selected for this research activity is a turbocharged, 4-cylinder, 1.6L passenger-car diesel engine equipped with an electronically actuated Variable Geometry Turbine (VGT) as well as an air-to-air Charge Air Cooler (CAC) and variable swirl flaps in its intake ports. The engine is equipped with two cooled EGR loops, a high and a low pressure one, and, as far as the fuel management system is concerned, with a common rail injection system with 8-hole solenoid injectors (Denso G3S) capable of operating up to 2000 bar injection pressure. Furthermore, the engine is equipped with an aftertreatment system consisting of a close-coupled Diesel Oxidation Catalyst (DOC) and a Diesel Particulate Filter (DPF), flowed by a Selective Catalytic Reduction (SCR) system mounted in underfloor position in the vehicle configuration. However, it has to be pointed out that, since the focus of the present work was on the impact of HVO characteristics on the combustion process and on engine-out emissions, in the current experimental setup the SCR was removed and replaced by a calibrated throttle valve, to properly replicate the exhaust back-pressure level, while DOC and DPF were kept to allow the recirculation of a "clean" (i.e. an exhaust from which the particles have been almost completely removed by the DPF) exhaust through the LP EGR circuit. Further engine specifications can be found in Table 4, along with those of the measurement devices in Table 5, while a sketch of the engine and emission sampling layout is depicted in Fig. 4. The engine tests have been carried out at the dynamic test bench of the Energy Department of Politecnico di Torino. The test rig is equipped with a highly dynamic AVL APA100 dynamometer and with an AVL KMA4000 fuel flow meter for fuel consumption measurements. An AVL AMAi60 emission analyser was utilized to measure the concentrations of NO, NOx, HC, CO, CO_2, and O_2, sampling the exhaust gases upstream of the aftertreatment system.

As far as soot emissions are concerned, an AVL 415S G002 Smoke Meter (SM) was used to measure the Filter Smoke Number (FSN). The AVL correlation [30] was then used to convert FSN into a soot concentration.

An AVL X-ion system was employed to measure pressure traces in the combustion chamber of cylinder #3 by using a high frequency piezoelectric pressure transducer (AVL GU 13P) as well as a high frequency current clamp to measure the solenoid injector current command. The in-cylinder pressures were acquired and subsequently processed by means of AVL® IndiCom software.

Table 4
Test engine main characteristics.

Engine type	4-cylinder, EURO 6 diesel engine
Displacement	1598 cm^3
Bore x stroke	79.7 mm x 80.1 mm
Compression Ratio	16:1
Air management system	Single stage VGT- LP and HP EGR
Fuel management system	Common rail (Max rail pressure: 2000 bar)
Rated power	100 kW @ 4000 rpm
Rated torque	320 Nm @2000 rpm

Table 5
Precisions and linearities of the measuring instruments.

Measured Variable	Sensor	Precision	Linearity
Fuel Mass flow	AVL KMA 4000	0.1 %	–
Torque	AVL APA100	0.3 % full scale (525 Nm)	–
Filter smoke number (FSN)	AVL 415S	0.005 FSN+3% Meas.value	–
Gaseous emissions concentrations	AVL AMA i60	–	2 %
In-cylinder pressure	AVL GU 13P	–	0.3 % full scale

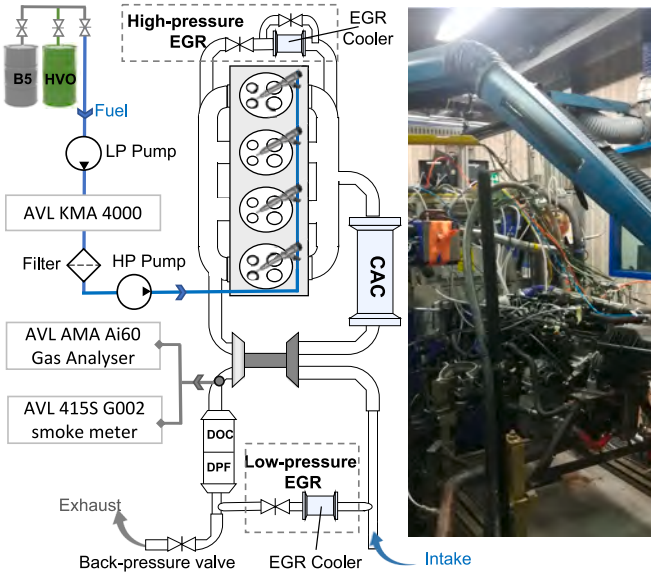

Fig. 4. Engine and emission sampling layout.

Finally, ETAS® INCA software was used to connect with the Engine Control Unit (ECU) to control, adjust, and record all engine operating parameters. Further details on the test rig and the equipment can be found in [31].

The test matrix consists of three different steady state operating points at 2000 rpm engine speed and 2, 5 and 8 bar Brake Mean Effective Pressure (BMEP), representative of low, medium, and medium–high load operation, respectively. A single injection strategy was used in all operating conditions to eliminate the interactions of pilot-main injections and to highlight the direct impacts of fuel characteristics more clearly on the ignition and combustion processes. Furthermore, a sensitivity analysis was carried out on the most influential parameters on the combustion process: EGR rate, Start of Injection (SOI) timing, and rail pressure were varied one by one on three different levels, as shown in Table 6. More specifically, when EGR sweep was performed, baseline SOI and Rail pressure (i.e., central value) were adopted. Prior to each test, the engine was initially warmed up for 30 min. Afterwards, for each operating point, the in-cylinder pressure and injection signals were measured for 50 consecutive cycles. Tests were repeated at least three times in different days to ensure a proper repeatability and data reported here below are average data.

4. Injection tests results and discussion

4.1. Hydraulic analysis

The hydraulic analysis was carried out over a set of 300 consecutive events in each operating condition, defined by fuel, rail pressure level and injection strategy. During each set of events, both the injected volume/mass and the injection rate for each single event were evaluated. Fig. 5 exhibits the mean injected mass and volume per shot obtained operating the injector at different rail pressure levels (500 bar, 1000 bar and 1500 bar) applying the single-injection strategy. In the same Figure, the CoV for the injected mass measured in each operating

Table 6
Engine test matrix.

Operating points	EGR (%)	SOI (°CA b TDC)	Rail pressure (bar)
2000 rpm x 2 bar BMEP	30 - 35 - 40	4.7 - 6.7 - 8.7	360 - 460 560
2000 rpm x 5 bar BMEP	24 - 28 - 32	5.8 - 7.8 - 9.8	450 - 650 - 850
2000 rpm x 8 bar BMEP	19 - 22 - 25	6.0 - 8.0 - 10.0	640 - 840 - 1040

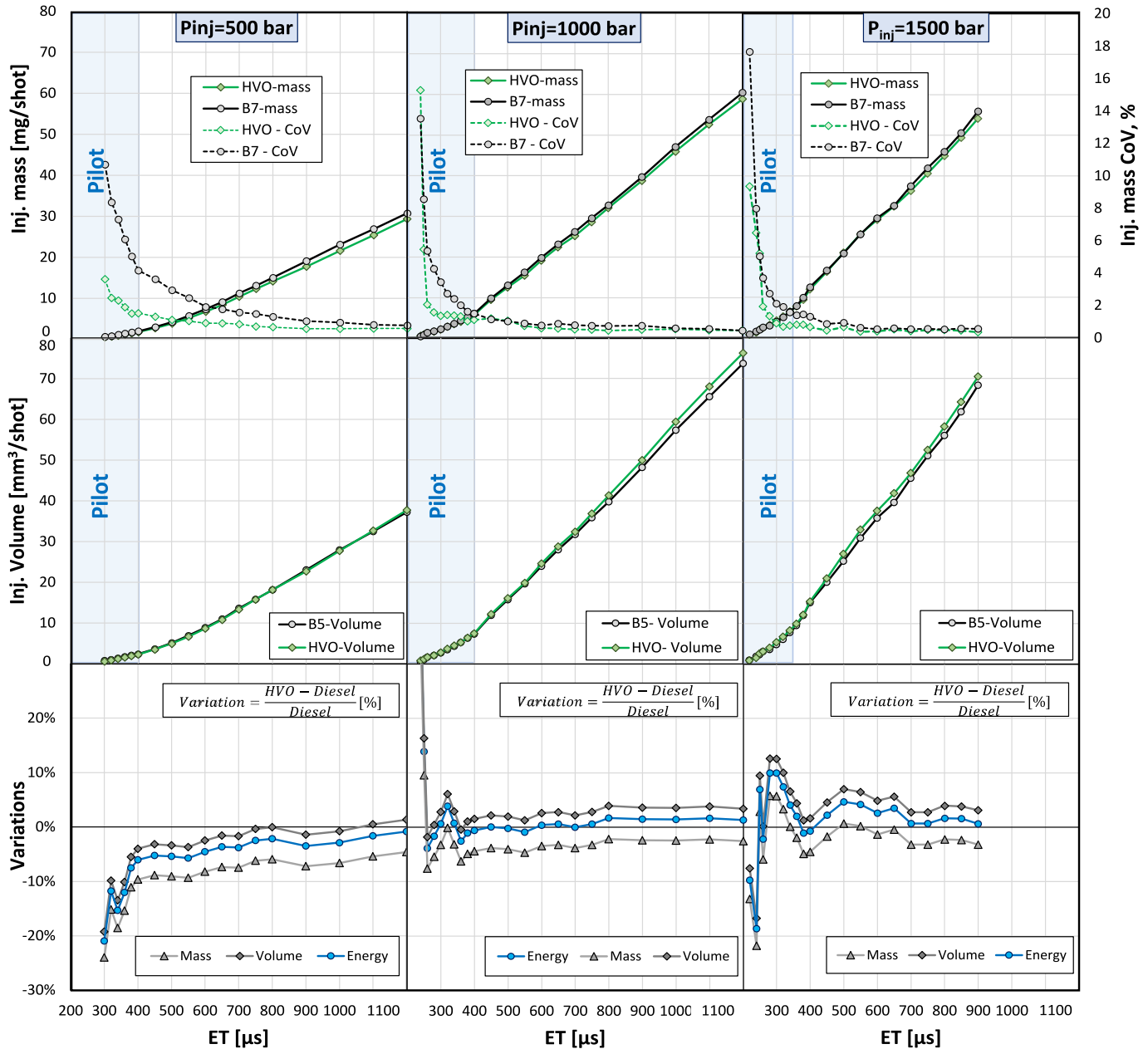

Fig. 5. Mean injected mass (with corresponding CoV) and volume and variations in values of mass, volume, and energy for HVO and B5 with a single injection strategy at P_{inj} = 500 bar, 1000 bar and 1500 bar.

condition is also reported. The shaded areas evidence the injector actuation duration range typically used for pilot injections. In the third row, the relative gap of HVO mean injected mass, volume, and energy with respect to B5 is depicted; the corresponding gap for the energy supplied by the injector to the combustion chamber can be evaluated considering the different energy content per unit mass (LHV_{HVO}=44.35 MJ/kg vs. LHV_{B5} = 42.65 MJ/kg) of the considered fuels.

As can be seen, for moderate rail pressure levels (P_{inj} = 500 bar) for relatively short injector actuations the HVO mean injected volume is consistently smaller, with the gap to B5 being more than 10 % for typical pilot conditions; only for actuation durations longer than 0.7 ms the gap of HVO to B5 can be considered marginal. Correspondingly, the difference in terms of energy introduced in the cylinder is significant for the entire range of the explored injector actuation duration. For higher pressure (P_{inj} = 1000 bar and, mostly, for P_{inj} = 1500 bar) the trend is different: the injected volume is generally slightly higher for HVO, as expected for the lower viscosity of HVO with respect to B5 fuel [32] (about – 10 %). At the same time, taking into account the lower density and the higher energy content of HVO with respect to B5, the resulting gap of energy supplied to the combustion chamber per injector actuation is completely recovered for intermediate injection pressure levels (P_{inj} = 1000) and becomes positive for P_{inj} = 1500 bar, particularly for short injector actuations. The observed differences in terms of mean injected volumes per shot can be better analysed in terms of injection rate time-profiles. The analysis of the instantaneous flow rate allows capturing the effects of the fuels characteristics (density, viscosity, and bulk modulus) on the transient and static flow phases of the injection event, that clearly can result in different trends for respectively short (pilot-like) and long injector actuations. In Fig. 6 the injection rate profiles measured for P_{inj} = 500, 1000 and 1500 bar are reported (for the sake of clarity, for each operating condition only the mean time-history obtained in the 300 consecutive injection events is presented).

As can be seen, for P_{inj} = 500 bar the HVO injection rate profiles are characterized by a slower rise in the injector opening phase, possibly as

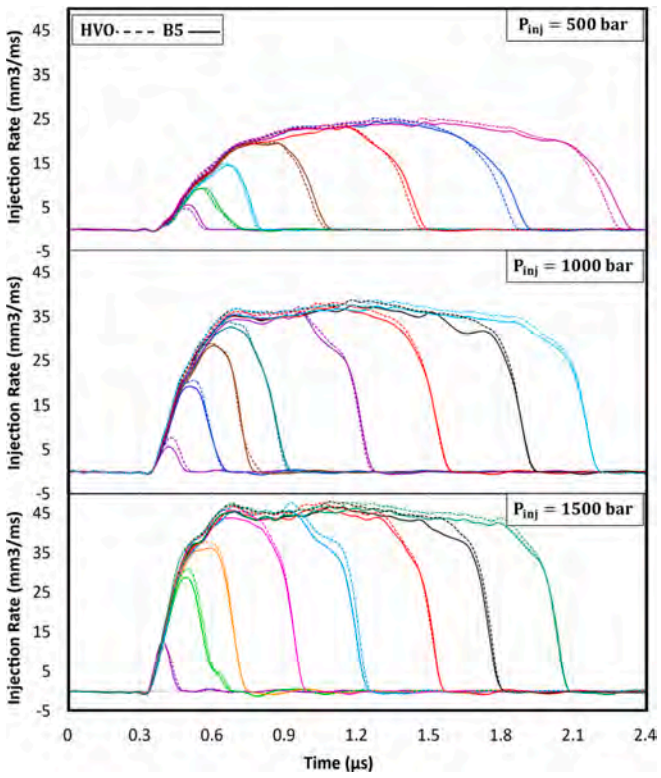

Fig. 6. Injection rate profiles for single actuation strategy, at Pinj = 500 bar, 1000 bar, and 1500 bar; time referred to injector current start.

an effect of a slower displacement for the nozzle needle (as also noted in [32]) resulting in a reduced peak flow rate with respect to B5 for short injection events, during which a static flow condition is not attained. This behaviour is likely to be ascribed to the effects exerted by the fuel characteristics on the pressure time-history in the injector control chamber.

When the injector current time is long enough (more than 0.6–0.8 ms) to allow a significant needle rise, the flow through the nozzle is no longer controlled by the needle position and the lower HVO viscosity causes the peak instantaneous injection rate to be higher for HVO. Finally, when the injector current ends, the injection rate profile for HVO is evidently shortened, possibly as a consequence of a faster needle descent to its seat determined by the pressure time-profile in the injector control chamber. Globally, for moderate injection pressure levels, the peculiar HVO characteristics cause a reduction of the injected volume and a shortening of the injection process, even if higher peak injection rates can be detected for long injection events. Clearly, this behaviour at moderate injection pressure levels could have significant effects in terms of actual injection rate profile with complex, multi-event injection strategies.

With high injection pressure levels, the injection rate profiles for HVO and B5 are very similar during both the injector opening and closing transients, possibly related to very similar needle lift time histories, leading to a very similar duration for the injection event. Conversely, the effects of the fuel characteristics in the phase in which the flow is not controlled by the needle position can be clearly observed, causing the instantaneous flow rate to be higher for HVO in steady flow conditions. As a result, in these conditions the injected volume per shot is increased with HVO with no substantial effects in terms of injection rate duration.

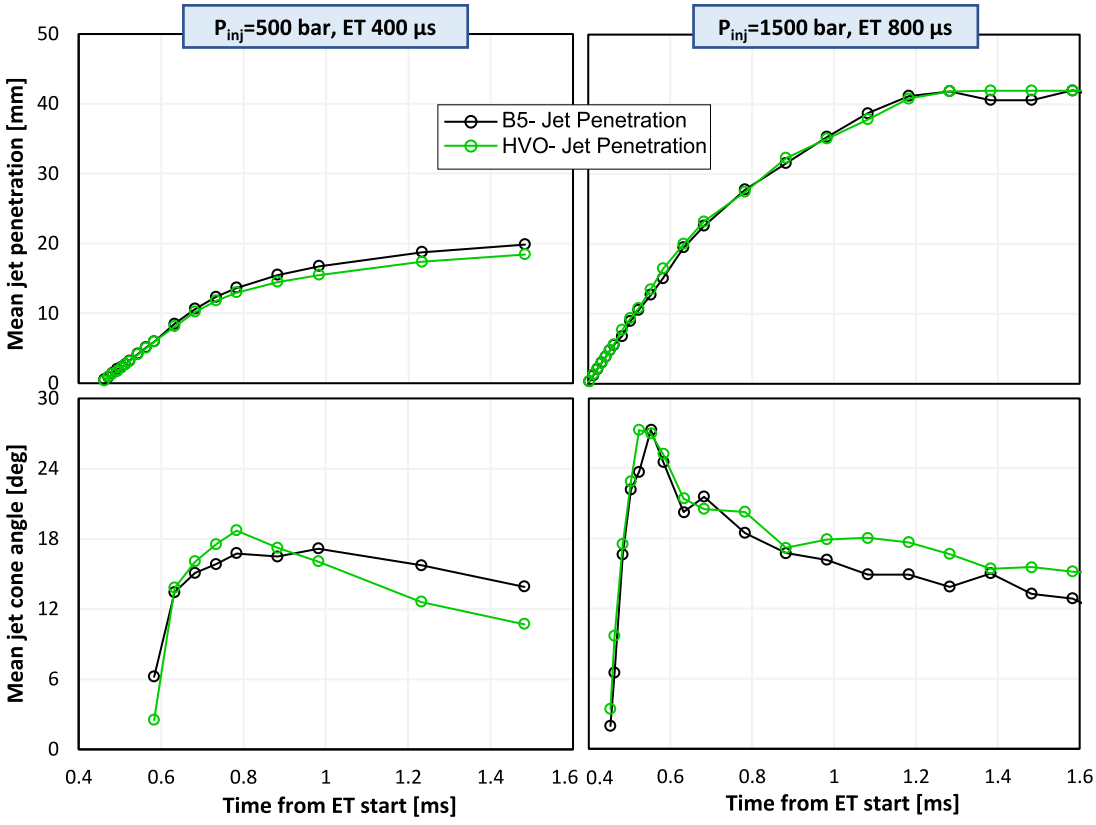

Fig. 7. Spray tip penetration and cone angle for P_{inj} = 500 bar, ET = 400 μs and P_{inj} = 1500 bar, ET = 800 μs.

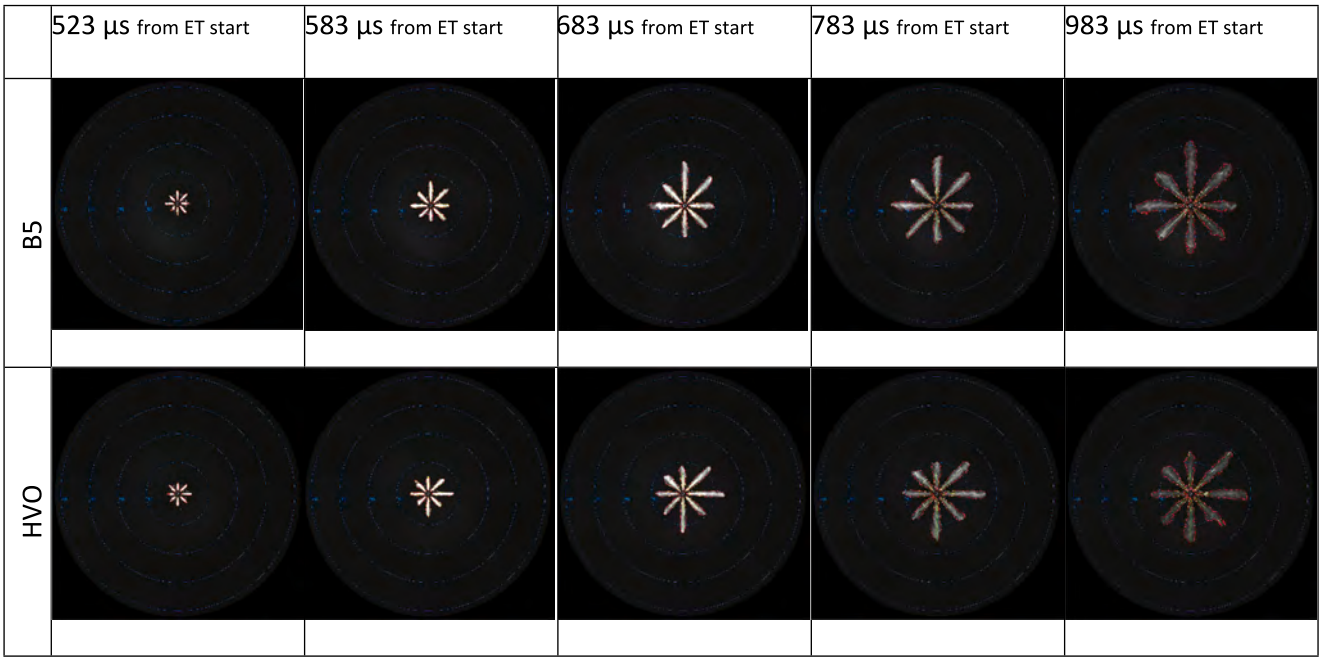

Fig. 8. Spray development for P_{inj} = 500 bar, ET = 400 µs. Timings from Start of Injector current.

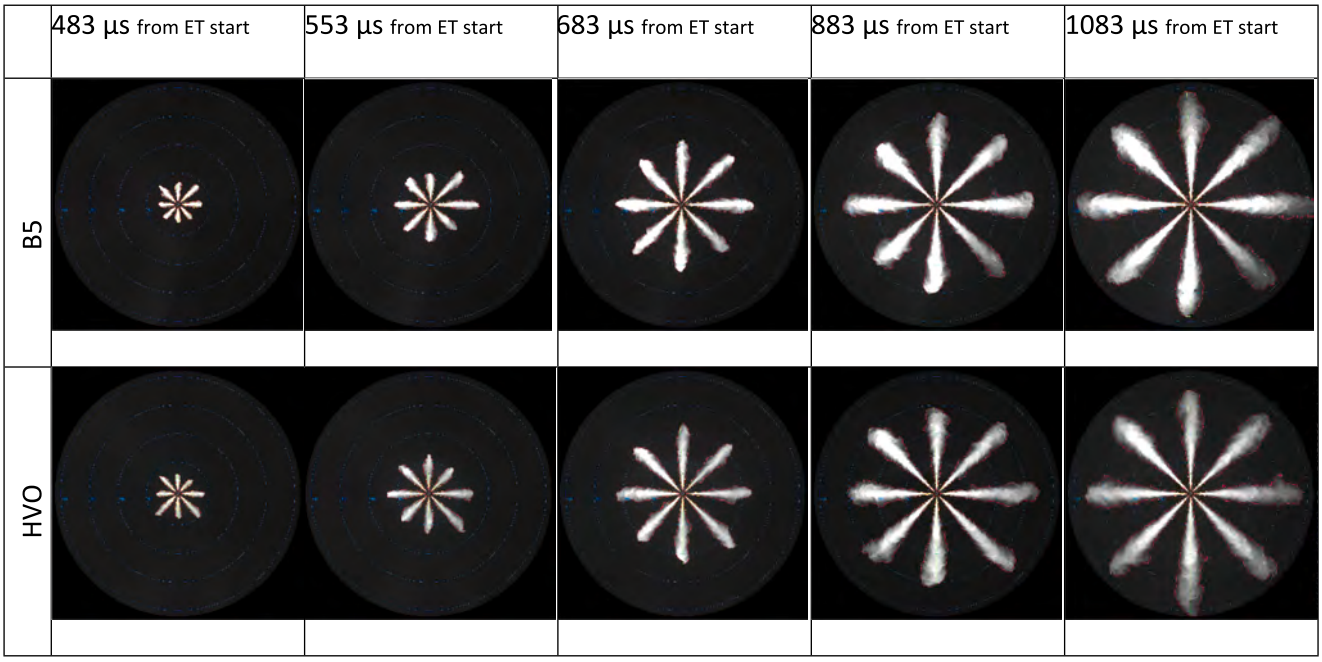

Fig. 9. Spray development for P_{inj} = 1500 bar, ET = 800 µs. Timings from Start of Injection current.

4.2. *Imaging analysis*

The HVO and B5 sprays development was investigated by imaging in high counter-pressure conditions with rail pressure ranging among 500 and 1500 bar, with energizing time varied respectively from 400 µs to 800 µs and from 250 µs to 800 µs. The spray tip penetration and cone angle plots for P_{inj} = 500 bar, ET=400 µs and P_{inj} = 1500 bar and ET=800 µs are reported in Fig. 7. The reported quantities are averaged over 30 repetitions per timing and over the 8 jets; on the right, the CoV of the obtained results are also reported. The sample pseudo sequences (according to the ensemble-average approach, each acquired image pertains to a different injection event) of the obtained results are reported in Fig. 8 for P_{inj} = 500 bar and in Fig. 9 for P_{inj} = 1500 bar. In these frames, the spray boundary detected by the image analysis procedure and used for quantitative determination tip penetration and cone angle curves of the 8 jets is reported (red line).

From the analysis of the spray global shape in Fig. 8 and Fig. 9, it is evident how different can be the plume structure evolution for the different jets emerging from the nozzle, particularly with moderate rail pressure levels and relatively short events, during which completely steady flow conditions are not reached. This behaviour, typical of both VCO (Valve Covering Orifice) and micro-sac nozzle, is normally considered to be produced by some needle side deviation during the injector opening phase [25] and is commonly less evident for higher

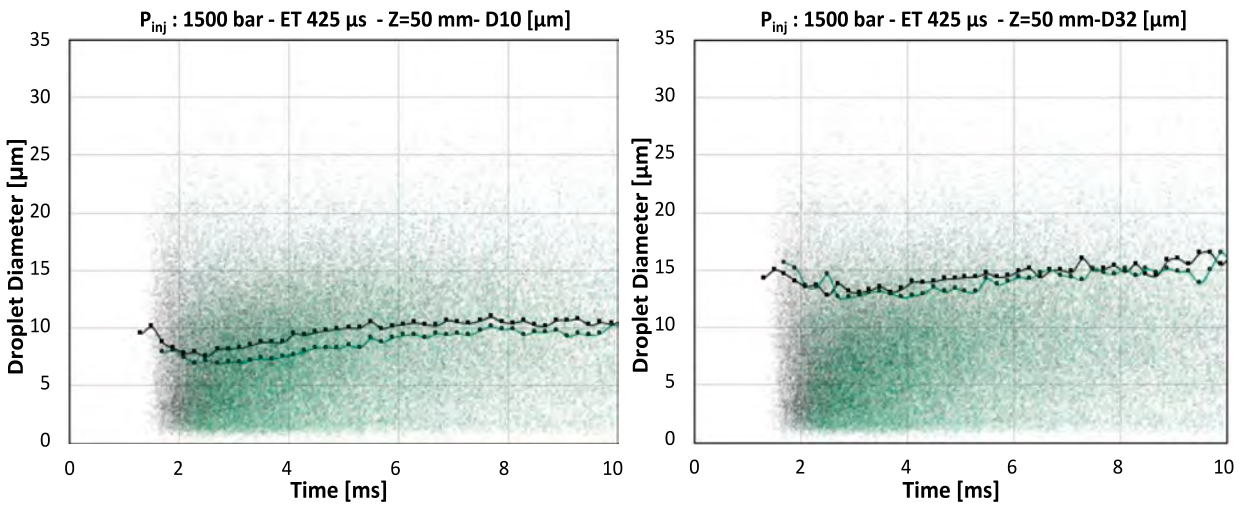

Fig. 10. Raw sizing data in X=0; Y=10; Z=50 mm for Pinj = 1500 bar, 18 mm3/shot. Individual drop values (grey and light green dots for diesel and HVO, respectively) and time-binned (0.1 ms) mean diameter values (in solid lines) of D10 (right) and D32 (left). (For interpretation of the references to colour in this figure legend, the reader is referred to the web version of this article.)

injection pressure levels and longer injection events, when the steady flow condition is reached, and the needle position is no longer affecting the fuel flow through the nozzle holes (Fig. 9).

Similar values in term of mean jet penetration were observed for HVO and B5 at P_{inj} = 500 bar up to 0.7 ms from the current start. Later a significantly lower penetration was observed for HVO, with an overall difference of about 1.5 mm at the latest timing; the advanced injector closure and the reduced injected volume for HVO observed in the hydraulic analysis (Fig. 6) can play a significant role. In terms of mean jet angle in the same operating conditions, the observed trend is similar among HVO and B5 sprays: the measured values evidenced initial values in the range 15 deg to 20 deg, followed by a decreasing trend, more evident for HVO, again possibly due to the advanced injection end. For the higher rail pressure level and longer injection duration (P_{inj} = 1500 bar, ET=0.8 ms) the obtained mean penetration curves are almost identical, and only minor differences were observed also in terms of jet cone angle. In these conditions, as evidenced by the analysis of Fig. 7, the overall spray development seems very similar among HVO and B5, as also suggested by the fact that the hydraulic analysis evidenced how the injected volume is only slightly higher for HVO and, mostly, the injection timing and duration is almost un-affected by switching from B5 to HVO. Consequently, in high rail pressure conditions, no significant differences in terms of spray evolution can be expected from the use of HVO.

4.3. Drop sizing and velocity

Sizing and velocity characteristics of drops were analysed along two orthogonal traverses over a plane 50 mm downstream the nozzle exit and crossing in the nominal projection of the jet axis on the examined plane. In each measurement station in the traverses, valid data pertaining to 315 consecutive shots were collected, using a 20 ms long time-window starting from the injector current start. The same test chamber conditions used for the above discussed imaging analysis were used. The PDA measurements were carried out for P_{inj} = 500, 1000 and 1500 bar with ET values corresponding to 18 mm^3/shot for all injection pressure levels and for both B5 and HVO. An example of the obtained raw sizing data is reported in Fig. 10, were the individual drop diameter values along with the trend of the mean diameter is reported for HVO and B5 with P_{inj} = 1500 bar.

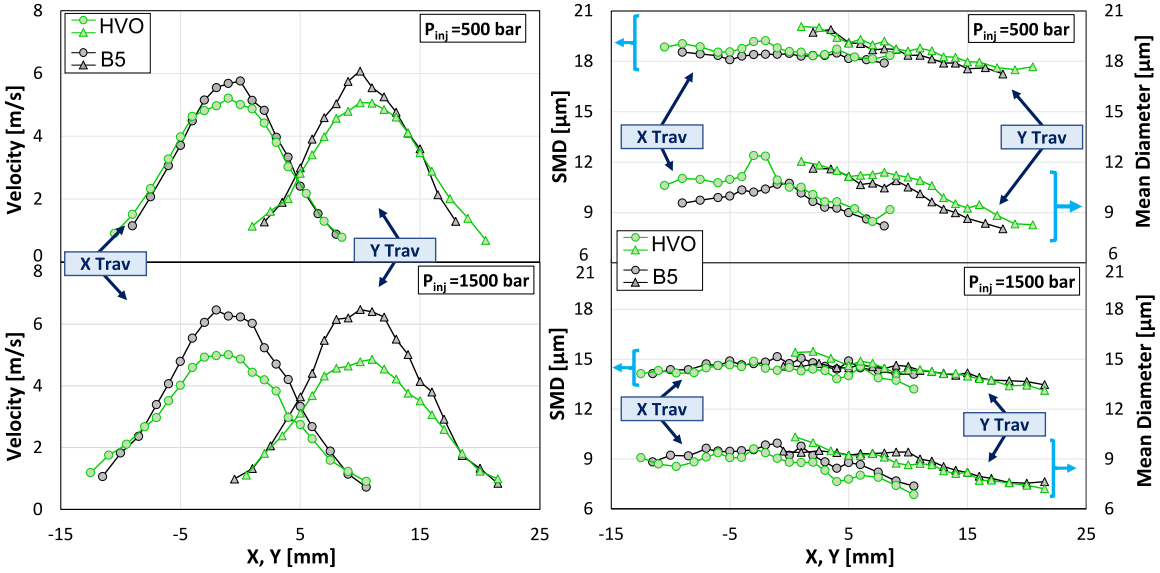

Fig. 11. Mean drops velocity, diameter and Sauter diameter along X and y traverses @ Z=50 mm for P_{inj} = 500 bar and 1500 bar, 18 mm^3/shot.

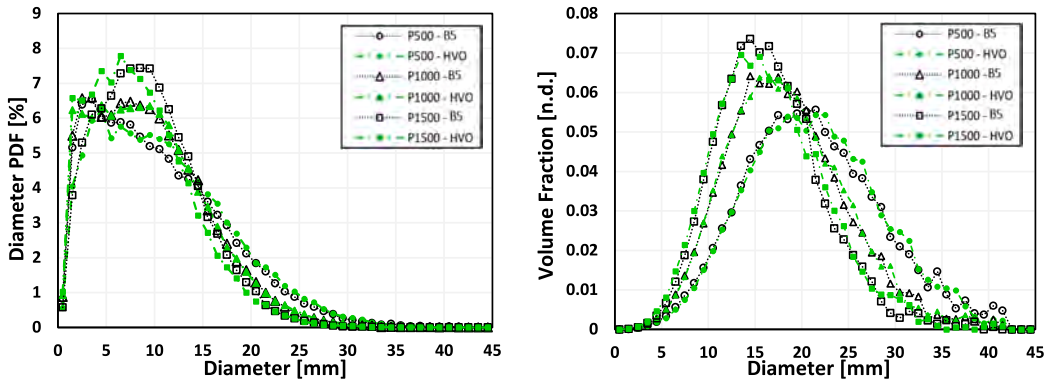

Fig. 12. Drops diameter probability density function and volume fraction distribution in X=0; Y=10; Z=50 mm for P_{inj} = 500, 1000 and 1500 bar, 18 mm^3/shot.

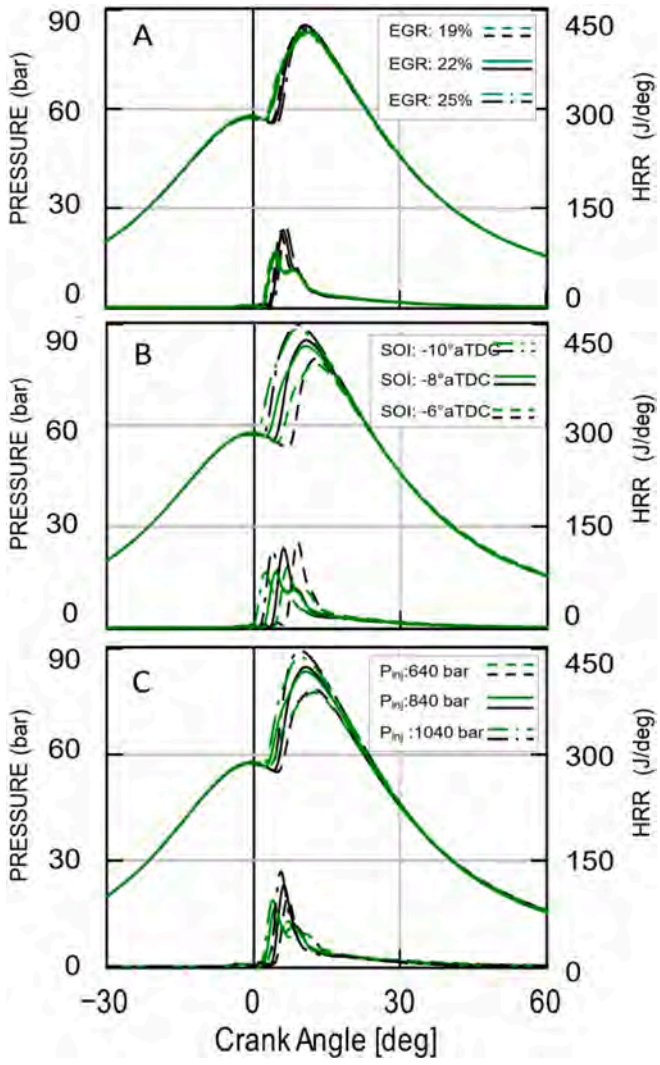

Fig. 13. In-cylinder pressure and heat release rate for EGR sweep (A), SOI sweep (B) and injection pressure sweep (C) at 2000 rpm, 8 bar BMEP.

As can be seen, in the considered operating condition droplets approach the measuring station about 1.8 ms, with the jet bulk being composed of drops featuring a mean diameter in the range of 7 to 9 μm (slightly lower for HVO). After about 4 ms from the ET start, the jet tail passes through the measuring station, with the mean diameter (D10) increasing to the final value close to 10 μm for B5 but slightly lower for HVO and the SMD close to 15 μm for both the fuels.

Considering the time-window from 0 to 20 ms, the mean drops velocity and sizing value pertaining to the entire injection process are reported in Fig. 11 for both the X and Y measuring traverses. The jet shape and mean drop velocity values are quite similar among HVO and B5 for both the analysed traverses, with some non-negligible differences observed only for the jet central positions.

In terms of drop sizing, slightly a-symmetrical mean diameter and Sauter mean diameter profiles were observed for both fuels along the X and Y traverses, suggesting in any case a very similar jet structure. However, at low injection pressure the mean diameters of HVO droplets are generally higher than the mean diameters of B5 droplets suggesting a better atomization for B5 at low injection pressures. By increasing the injection pressure, the HVO droplets take smaller sizes with respect to diesel that could account for the further lower mean velocity in the same positions.

In Fig. 12 drops diameter probability density function and the corresponding volume fraction distribution in the X and Y traverses intersection are reported for the three analysed injection pressure levels.

As can be seen, the main effect on the statistical distribution of drops diameter is exerted by the rail pressure level, with the PDF profile pertaining to 500 bar evidencing a significant number of droplets featuring diameters in excess of 35 μm, while for P_{inj} = 1500 bar the PDF upper limit seems to be around 30 μm. At the same time, the peak of the PDF profile increases from 2.5 μm to 7.5 μm, probably as an effect of promoted secondary break-up phenomena with increased drops velocity due to the increase of the injection pressure.

Globally, the volume fraction distributions are deeply affected by the injection pressure level, with the peak decreasing from 22 μm to 15 μm. The effect of the fuel composition does not seem to evidence a levels, confirming a substantial neutrality of HVO in terms of injection process management.

5. Combustion tests results and discussion

The results of the engine test will be presented and discussed in the following sections, starting with the medium–high load operating condition (Fig. 13 and Fig. 14), to then move to the medium load (Fig. 15 and Fig. 16) and finally to the low load (Fig. 17 and Fig. 18).

Moreover, the average differences between the two fuels in terms of main combustion parameters, consumption and pollutant emissions are summarized in Tables 7 and 8 here below to provide to the reader an overall summary of the results.

Finally, as far as the uncertainty of the results is concerned, error bars were added which indicate the maximum and minimum values for each test across the three repetitions in an additional figure set (Figures S1-3) in the supplementary file, so to maintain a good readability of the plots in the main text.

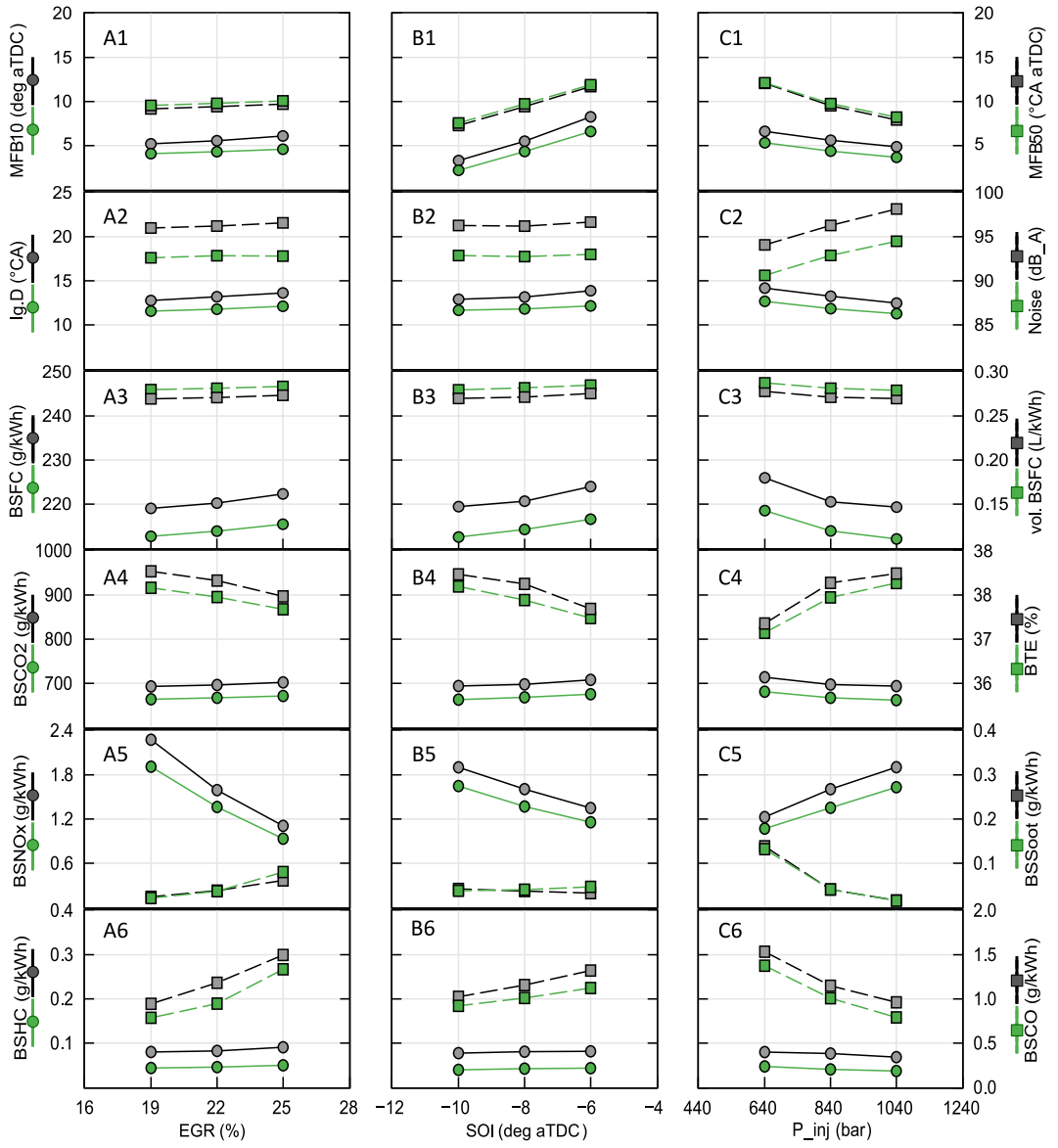

Fig. 14. Combustion timing parameters MFB10 and MFB50, ignition delay and Combustion Noise, BSFC and Vol.BSFC, specific emissions and BTE for B5 (in black) and HVO (in green) for EGR sweep (column A), SOI sweep (column B) and injection pressure sweep (column C) at 2000 rpm, 8 bar BMEP. (For interpretation of the references to colour in this figure legend, the reader is referred to the web version of this article.)

5.1. *Medium-high load operating conditions*

The results of the medium–high load tests (at 2000 rpm and 8 bar BMEP) are reported in Fig. 13 and Fig. 14.

From in-cylinder pressure and heat release rate traces shown in Fig. 13, it is evident that the higher cetane number of HVO results into a shorter ignition delay (see also Figure 14 -A2, B2 and C2, where the ignition delay is about 1.5° CA shorter for HVO, on average) and in a lower intensity of the premixed burn phase. The latter, in turn, leads to a lower rate of pressure rise and, as a consequence, to a lower combustion noise (3.5 dB_A lower for HVO on average, as shown in Figure 14 -A2, B2 and C2). Also, NOx emissions are lower (about 0.24 g/kWh lower for HVO, on average, as shown in Figure 14 –A4, B4 and C4), due to the lower peak in the heat release rate, which leads to lower peak temperatures.

Coming back to the combustion process (Fig. 13), due to shorter ignition delay and a lower intensity of the premixed burn, HVO combustion reaches MFB10 values earlier than B5 (about 1.5° CA earlier, on average, see also Figure 14 –A1, B1 and C1), to then show MFB50 positions almost identical to B5 due to the more intense premixed combustion phase of this latter (again, see Figure 14 –A1, B1 and C1). Due to the almost identical combustion phasing, the two fuels then exhibit only marginal differences in terms of BTE (less than 1 %, see Figure 14 –A4, B4 and C4). However, despite these modest differences in BTE, the higher LHV of HVO (see Table 1) leads to gravimetric fuel consumption values about 3 % lower, on average, than B5 (see Figure 14 –A3, B3 and C3). Nevertheless, from the final user's perspective for LD applications, the volumetric fuel consumption should be considered, and, in this case, the higher LHV of HVO (+4.0 % with respect to B5) cannot compensate for its lower density (−6.4 % with respect to B5, see Table 1), thus leading to a 3 % higher volumetric fuel consumption for HVO (see again Figure 14 –A3, B3 and C3).

Furthermore, as far as specific CO_2 emissions are concerned, HVO shows values which are, on average, 4.5 % lower than B5 ones, also thanks to its higher H/C ratio. This 4.5 % Tank-to-Wheel reduction, summing up with the previously mentioned 81 % reduction on a Well-to-Tank basis, will therefore lead to an impressive 85 % reduction on a WTW basis.

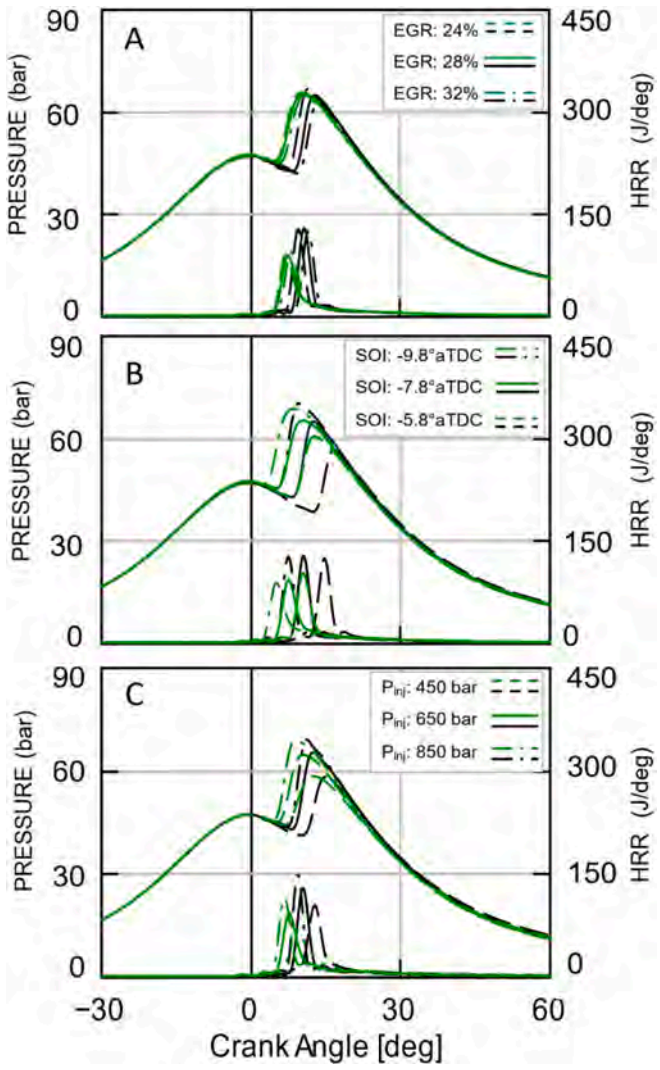

Fig. 15. In-cylinder pressure and heat release rate for EGR sweep (A), SOI sweep (B) and injection pressure sweep (C) at 2000 rpm, 5 bar BMEP.

Finally, the shorter ignition delay and, consequently, the shorter time available for mixing, produce a slight increase of soot emissions (about 6 %) for HVO (see Figure 14 –A5, B5 and C5), while significant reductions in terms of specific HC and CO emissions (on average 46 % and 14 % lower than those of B5, respectively) can be observed (see Figure 14 –A6, B6 and C6) thanks to the shortened ignition delay and improved combustion quality.

Effects of EGR

In the medium–high load operating condition, a variation in the EGR rate produces only limited changes in the quality and timing of the combustion process for both fuels (trends shown in Fig. 13-A and Figure 14-A1 and A2 are almost flat). Moreover, also the reductions in combustion noise, specific CO_2 emissions, and BSFC which can be observed for HVO compared to B5, remain almost constant for all EGR levels. As far as pollutant emissions are concerned, both fuels exhibit similar sensitivity to EGR rate variations, with differences in HC, CO, and NOx emissions which are almost constant between the two fuels for all EGR rates. Only at the highest EGR rate of 25 %, slightly higher soot levels for HVO were measured, likely due to the shorter time available for mixing (because of the shorter ignition delay) for HVO compared to B5.

Effects of injection timing

The SOI variations explored induce comparable changes in both the quality and timing of the combustion process for both HVO and B5 fuels, as evidenced by the similar trends depicted in Fig. 13-B and Figure 14-B1 and B2. Consequently, nearly all pollutants exhibit similar sensitivities to the SOI variations for both fuels.

Effects of injection pressure

Both HVO and B5 show nearly equal sensitivities to injection pressure variations, with differences between the two fuels remaining almost constant for all the injection pressure levels explored.

5.2. Medium load operating conditions

Fig. 15 and Fig. 16 report the results of engine tests at 2000 rpm and medium load, i.e., 5 bar BMEP, including again a sensitivity analysis to EGR rate, SOI timing, and injection pressure. From the in-cylinder pressure and HRR traces in Fig. 15, it is immediately perceivable that the differences between the two fuels are much more evident compared to the higher load operating condition which was previously discussed (see Fig. 13).

Comparing the timing of the HVO combustion phases at medium load in Fig. 15 (see also Figure 16-A1, B1 and C1) with those of medium–high load (Fig. 13 and Figure 14-A1, B1 and C1), it can be seen that at 5 bar BMEP the combustion phasing for HVO is more advanced in all cases, despite the almost identical SOI timing for both operating conditions (SOIs are just 0.2°CA earlier for medium load operation). On average, at 8 bar BMEP, the MFB10 for HVO combustion phase occurred 1.2°CA earlier than for B5, with the same MFB50 timing for both fuels. Instead, at 5 bar BMEP, the MFB10 and MFB50 for HVO combustion occurred 2.7°CA and 2.1°CA earlier than for B5, respectively. Fig. 15 and Figure 16-A2, B2 and C2 also clearly show the shorter ignition delays of HVO in comparison to the higher load operating condition (Fig. 13 and Figure 14-A2, B2 and C2), as at this lower load, the higher cetane number of HVO is playing a more important role.

As a consequence, despite the lower intensity of the premixed combustion phase for HVO in all cases, the decrease in HVO combustion noise is slightly less pronounced with respect to higher load operation, since the HVO combustion phase starts earlier and reaches higher peak pressures than those of B5, thus causing higher pressure rise rates ($dP/d\theta$) for HVO at lower loads.

The lower fuel consumption of HVO at the medium load is more pronounced comparing to the medium–high operating point (Figure 16-A3, B3 and C3) as a sign of improved efficiency, thanks to the better combustion phasing with HVO. The loss of about 1 % on average in HVO brake thermal efficiency at medium–high operating points is almost recovered in lower medium load operation (Figure 16-A4, B4 and C4). Similarly, to the medium–high load operation, about 4 % reductions in CO_2 emissions can be achieved with HVO (Figure 16-A4, B4 and C4).

Moreover, the shorter ignition delay of HVO provides less time available for the air fuel mixing process, thus leading to higher specific soot emissions for HVO in all cases (see Figure 16-A5, B5, C5, in good agreement with results reported in literature as in [23]). Regarding the NOx emissions, similarly to the higher load operation, about 15 % reductions for HVO were achieved at medium load operation.

Finally, at 5 bar BMEP, HVO combustion resulted in even more significant reductions in HC and CO levels (−56 % and −50 %, respectively) with respect to 8 bar BMEP operating points (see Figure 16-A6, B6, C6 and Table 8), again, thanks to the better ignition quality of HVO, which is likely to play a more important role at lower load.

Effects of EGR

As for the higher load operating point, also at medium load operation, both fuels show similar sensitivities towards EGR in terms of combustion timings, noise, and efficiency, as well as of fuel consumption and CO_2 emissions.

Differently, HVO exhibits a lower sensitivity than B5 to EGR in terms of BSNOx, and on the contrary, a higher sensitivity for soot (Figure 16-A5). The higher soot increase for higher EGR rates for HVO can be attributed to the lower impact the EGR increase has on the increase of the ignition delay (which is in turn allowing more time for air fuel

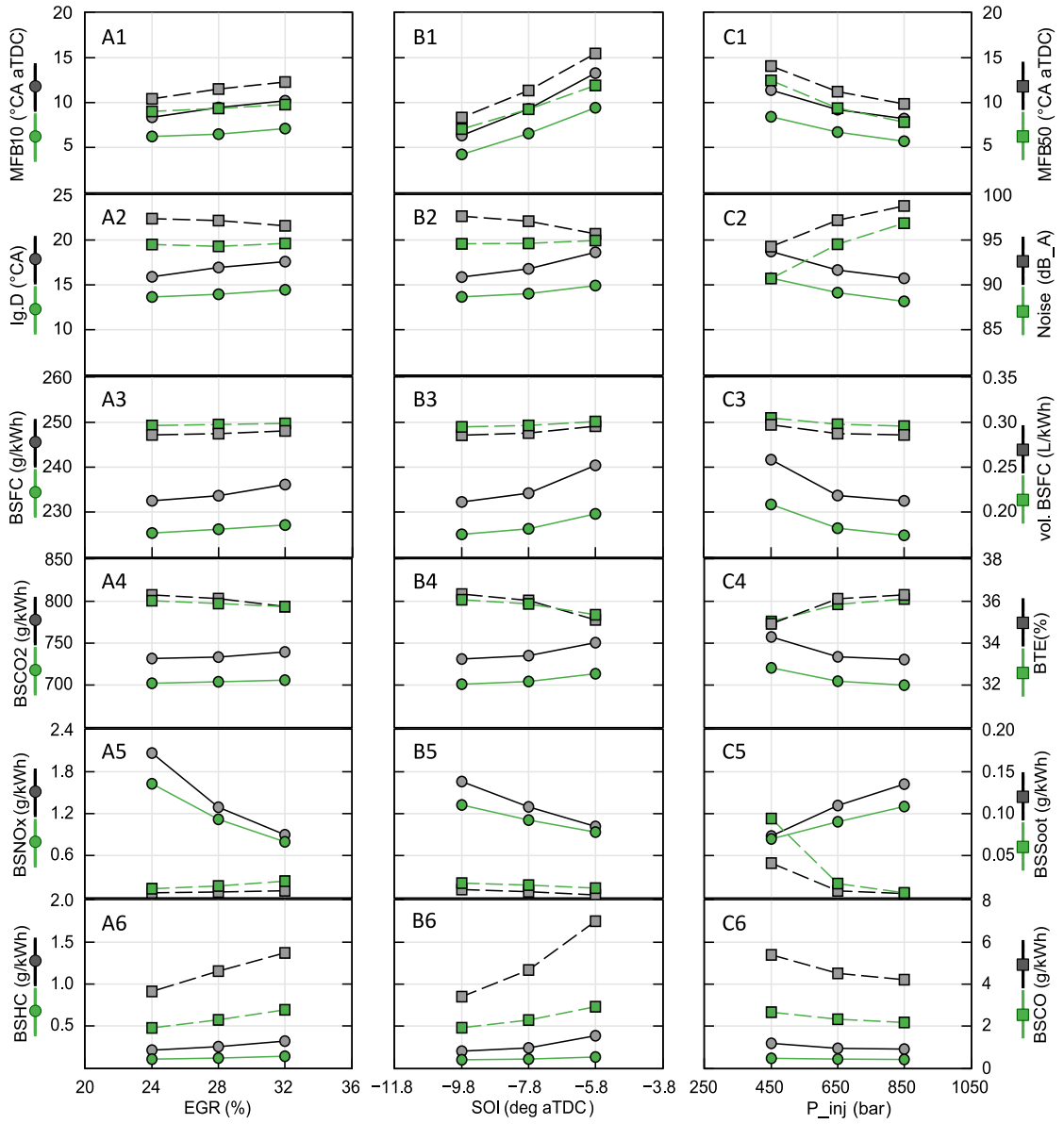

Fig. 16. *Combustion timing parameters MFB10 and MFB50, ignition delay and Combustion Noise, BSFC and Vol.BSFC, specific emissions and BTE for B5 (in black) and HVO (in green) for EGR sweep (column A), SOI sweep (column B) and injection pressure sweep (column C) at 2000 rpm, 5 bar BMEP.* (For interpretation of the references to colour in this figure legend, the reader is referred to the web version of this article.)

mixing) due to the higher reactivity of the fuel.

Finally, as depicted in Figure 16-A6, HVO also exhibits a lower sensitivity than B5 to EGR in terms of BSHC and BSCO, again likely thanks to the better ignition quality of HVO.

Effects of injection timing

From the results reported in Fig. 15-B and Figure 16-B1, B2, B3 and B4 it can be concluded that HVO combustion is less sensitive than B5 combustion to SOI timing.

Another notable observation, highlighted in Figure 16-B6, is the lower sensitivity of HVO to SOI timing in terms of HC and CO emissions. Generally, HC formation exhibits a close correlation with ignition delay. By advancing SOI, the combustion delay for B5 is reduced by 3°CA, whereas for HVO, it decreases by about 1°CA only. Consequently, BSHC emissions for HVO are less sensitive to SOI timing. Similar trends can be observed for BSCO emissions, although the primary influencing factor on BSCO is not ignition delay but rather the local equivalence ratio, which is more significantly improved for B5 than for HVO with advanced SOI timing.

Effects of injection pressure

First of all, it has to be pointed out that increasing injection pressure will reduce ignition delay and combustion duration for both fuels at medium load (5 bar BMEP) in a more pronounced way than at medium–high load (8 bar BMEP). Moreover, HVO appears to be more sensitive than B5 to injection pressure increase particularly for soot emissions, as clearly shown in Figure 16-C5, where HVO soot emissions, more than 100 % higher than B5 ones at 450 bar injection pressure, can be reduced to almost identical values to B5 ones at 850 bar injection pressure.

This different sensitivity can be explained as follows. Low-pressure injection (450 bar) results in slightly bigger droplets for HVO (see Fig. 11), which alongside with HVO shorter ignition delays due to its higher cetane number, worsen the fuel–air mixing and leads to higher soot formation for HVO (in good agreement with results reported in literature [33] overcoming the benefits which could be expected in terms of reduced soot formation thanks to the lack of aromatics in the HVO fuel molecules. On the other hand, at higher injection pressures

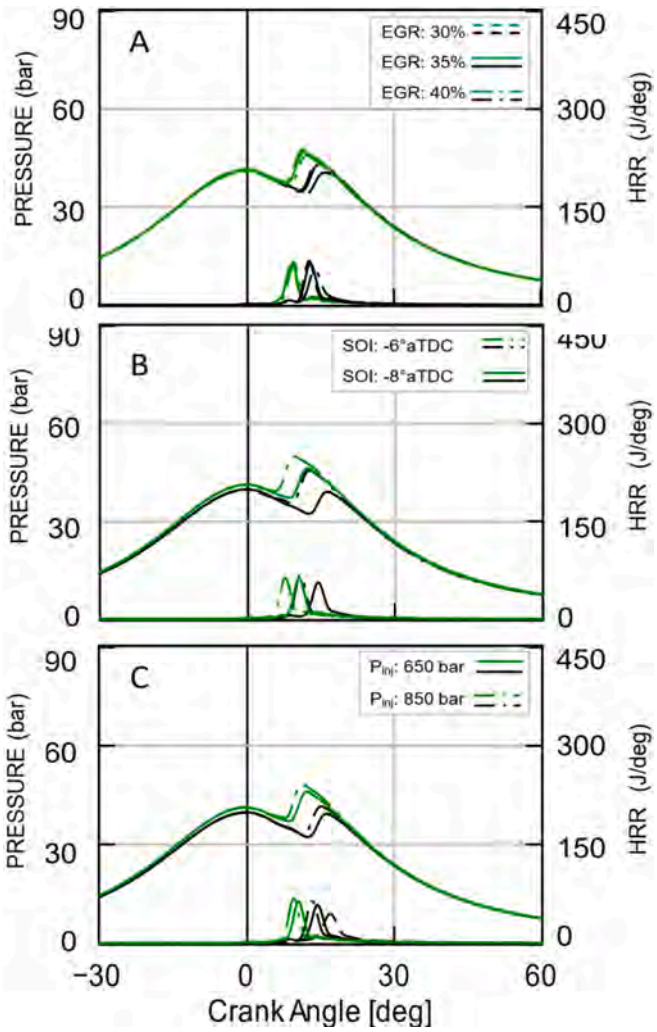

Fig. 17. In-cylinder pressure and heat release rate for EGR sweep (A), SOI sweep (B) and injection pressure sweep (C) at 2000 rpm, 2 bar BMEP.

(850 bar) fuel atomization improves more for HVO than for B5 (as shown in Fig. 12), with at least a partial compensation of the adverse impact of the shortening of the ignition delay on the fuel–air mixing.

5.3. Low load operating conditions

Investigating low load operating conditions is critical since the effect of high cetane number is more pronounced [34]. Also, from the spray analysis reported in the previous section, it was found out that at low loads (i.e., at low ETs and injection pressures) the deviations of HVO injected volume and energy with respect to B5 are at their maximum levels. Thereupon, the main challenges for the usage of neat HVO could be expected to be for low-load operations. Fig. 17 and Fig. 18 report the results of the tests carried out at 2000 rpm and 2 bar BMEP: it should be pointed out that, due to combustion instability issues, the range of the SOI and injection pressure values could not be fully explored. As the in-cylinder pressure and heat release rate traces in Fig. 17 indicate, in all cases, the shift of HVO combustion phase to earlier crank angles in comparison to B5 combustion phase is more evident with respect to medium–high and medium loads (8 and 5 bar BMEP – see Fig. 13 and Fig. 15). At low load operation, due to lower temperatures of the in-cylinder charge, the ignition delay for both fuels (Fig. 17, see also Figure 18-A2-B2-C2) is significantly longer than for higher loads (compare with Figure 14-A2, B2, C2 and Figure 16-A2, B2, C2), and, as a matter of fact, the effects of HVO higher reactivity are more evident.

The heat release traces in Fig. 17 also clearly show that the combustion process for both fuel is almost entirely made of a premixed combustion due to the injection of relatively small fuels quantities, reaching almost identical peak values, although with significantly different phasings. Consequently, comparable combustion noise levels were measured for both fuels (see Figure 18-A2, B2 and C2).

The shorter ignition delay of HVO allows a better combustion phasing, thus completely recovering the small BTE losses with reference to B5 (see Figure 18-A4, B4 and C4), which were measured at medium–high and medium loads. Therefore, at low-load operation HVO reaches the maximum improvements in BSFC (16.5 g/kWh or about 4 % lower than the BSFC of B5, on average, as shown in Figure 18-A3, B3 and C3). Finally, it has to be pointed out that HVO appears to be less sensitive than B5 to an injection pressure increase in terms of BSNOx (see Figure 18-C5), thus suggesting the possibility to achieve significant improvements as far as the NOx-soot trade-off is concerned.

As far as pollutant emissions are concerned, the reductions in NOx emissions for HVO with respect to higher-load operating conditions is less pronounced (about 9 % reduction, on average, see Figure 18-A5, B5, and C5, with respect to about 14.5 % reduction for medium–high and medium load conditions), due to the closer to TDC combustion phasing for HVO with respect to B5, leading to higher combustion pressures and temperatures for HVO.

On the other hand, although soot emissions show extremely low values in absolute terms for both fuels, a noticeable increase in HVO emissions is evident at low load: this can be attributed to the large reduction in ignition delay, which is in turn dramatically reducing the time available for air–fuel mixing, and, along with the worse fuel jet atomization at low injection pressures for HVO, leads to higher soot formation (in good agreement with results reported in literature [32]). Finally, the HVO specific HC and CO emissions reach their maximum reductions at this low-load operating condition (on average 70 % and 61 % lower than those of B5, respectively – see Figure 18-A6, B6, and C6) likely due to HVO better combustion efficiency.

Effects of EGR

The better ignition quality of HVO makes it less sensitive than B5 to EGR increase: the ignition delay of HVO remains almost constant at increasing EGR rates up to 40 %, while the combustion phasing just shows only moderate changes at high EGR levels (see Fig. 17-A and Figure 18-A1 and A2). Finally, as far as pollutant emissions are concerned, the lower sensitivity of HVO to the EGR rate allows the achievement of extremely low HC and CO emissions even for high EGR rates up to 40 %, for which B5 emissions significantly deteriorate (see Figure 18-A6).

Effects of injection timing

At this low-load operating condition, the most retarded injection timing (−4.7 aTDC) could not be explored due to severe combustion instability issues. Again, as it was already pointed out for EGR, HVO resulted to be less sensitive to SOI timing variations, and this could provide significant benefits in terms of HC and CO emissions, as shown in Figure 18-B6.

Effects of injection pressure

Similarly, to the previously described test case, also the lowest injection pressure (360 bar) could not be explored due to severe combustion instability issues. This instability was particularly notable for HVO, likely due to the large variations of injected quantities and to the significant worsening of the fuel jet atomization at low injection pressures, as shown in Fig. 5 and Fig. 11, respectively.

By increasing the injection pressure from 460 to 560 bar, both fuels demonstrate the same sensitivity in terms of almost all combustion parameters as well as emissions.

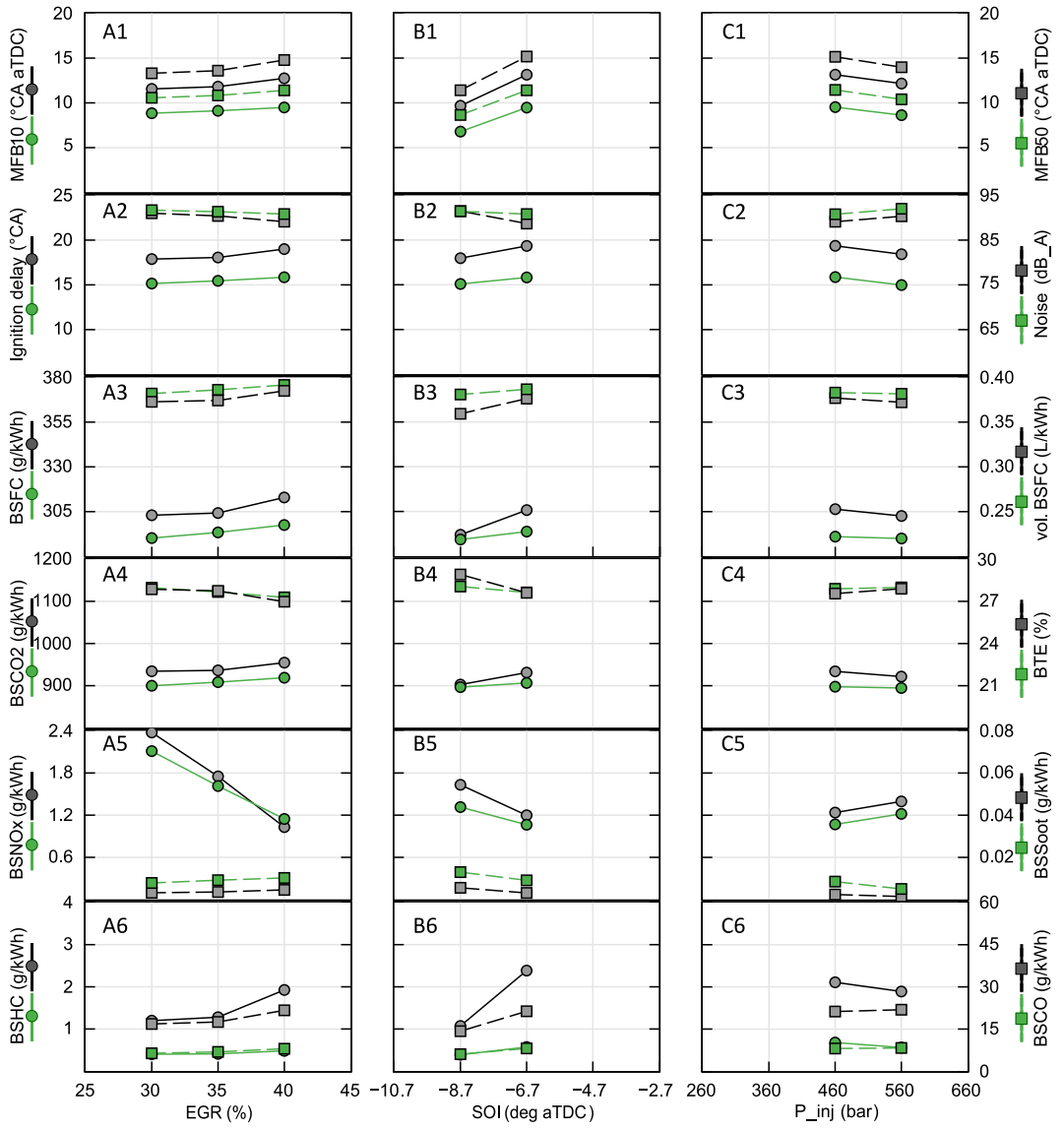

Fig. 18. Combustion timing parameters MFB10 and MFB50, ignition delay and Combustion Noise, BSFC and Vol.BSFC, specific emissions and BTE for B5 (in black) and HVO (in green) for EGR sweep (column A), SOI sweep (column B) and injection pressure sweep (column C) at 2000 rpm, 2 bar BMEP. (For interpretation of the references to colour in this figure legend, the reader is referred to the web version of this article.)

Table 7
Absolute differences (Δ = [HVO]-[B5]) of main combustion timing parameters and of Combustion Noise (average values on all test points) for 2000 rpm and 2, 5, and 8 bar BMEP.

rpm x bar BMEP	Ig. Delay [°CA]	MFB10 [°CA]	MFB50 [°CA]	Comb. Noise [dB_A]
2000 x 8	−1.4	−1.3	0.3	−3.5
2000 x 5	−2.8	−2.8	−2.1	−2.5
2000 x 2	−3.1	−3.2	−3.2	1.2

6. Conclusions

In this study, the main injection and combustion characteristics of neat Hydrotreated Vegetable Oil (HVO) as an alternative fuel for light-duty diesel engines have been analysed by means of an experimental approach based on a single injection strategy in both spray and engine laboratory tests, at low, medium, and medium–high load operating conditions. The choice to operate the engine with a single injection, although substantially deviating from the normally adopted multi-injection strategies, allowed to better highlight the effects of the different fuel characteristics on both fuel injection and combustion, as

Table 8
Percentage of variations (averaged on all test points) for efficiency, fuel consumption, and emissions for HVO with respect to B5.

rpm x bar BMEP	BTE	$BSFC_{grav}$	$BSFC_{vol}$	$BSCO_2$	*BSNOx*	*BSSOOT*	*BSHC*	*BSCO*
2000 x 8	−0.8	−3.1	3.5	−4.4	−14.6	5.7	−45.8	−13.9
2000 x 5	−0.3	−3.5	3.1	−4.3	−14.6	120.2	−56.3	−49.8
2000 x 2	0.0	−3.8	2.7	−2.9	−9.2	179.5	−69.6	−61.4
Overall average	**−0.4**	**−3.4**	**3.1**	**−4.0**	**−13.1**	**95.6**	**−56.2**	**−40.1**

well as on the interactions between the two processes.

The key findings can be summarized as follows:

- In terms of mean injected volume and mass per shot obtained operating the injector at different rail pressure levels (500 bar, 1000 bar and 1500 bar) with a single-injection strategy, for moderate rail pressure levels (Pinj = 500 bar) and for relatively short injector actuations the HVO mean injected volume is consistently smaller, with the gap to B5 being more than 10 % for typical pilot conditions, and only for actuation durations longer than 0.7 ms the gap of HVO to B5 can be considered marginal. Correspondingly, the difference in terms of energy introduced in the cylinder is significant. For higher pressure (Pinj = 1000 bar and, mostly, for Pinj = 1500 bar) the injected volume is instead generally slightly higher for HVO, and the resulting gap of energy supplied to the combustion chamber per injector actuation is completely recovered for intermediate injection pressure levels (Pinj = 1000) and becomes positive for Pinj = 1500 bar, particularly for short injector actuations.
- In terms of injection rate time-profiles, for moderate injection pressure levels, the peculiar HVO characteristics cause a reduction of the injected volume and a shortening of the injection process, even if higher peak injection rates can be detected for long injection events. With high injection pressure levels, the injection rate profiles for HVO and B5 are very similar during both the injector opening and closing transients, leading to a very similar duration for the injection event. Conversely, the effects of the fuel characteristics in the phase in which the flow is not controlled by the needle position can be clearly observed, causing the instantaneous flow rate to be higher for HVO in steady flow conditions. As a result, in these conditions the injected volume per shot is increased with HVO with no substantial effects in terms of injection rate duration.
- The effects of different hydraulic behaviour of HVO at low injection pressures is reflected in a shorter spray penetration and in a lower mean cone angle with relatively higher variations. At higher injection pressure levels, the spray evolution parameters become almost identical for both fuels.
- In general, HVO shows similar atomization properties to B5. However, at low injection pressure the mean diameters of HVO droplets are generally higher than those of B5 droplets. Again, at higher injection pressure levels, the spray atomization parameters become almost identical for both fuels, with smaller droplets for HVO.
- As far as combustion characteristics are concerned, the impact of HVO characteristics (and in particular of its higher Cetane Number) is more pronounced at low load operating conditions, while in medium–high loads the injection and combustion behaviours of the two fuels get closer to each other.
- With the single injection strategy, the higher cetane number of HVO always leads to significant shortenings of the ignition delay: at medium–high load and at medium load this leads to a lower peak of the heat release rate, and to a lower combustion noise. At low load, where most of the combustion process is occurring in the premixed phase, the shortening of the ignition delay does not cause significant reduction in the peak of the heat release rate, but rather a shift towards a more anticipated combustion. Moreover, such pronounced shortenings of the ignition delay also cause significant reductions of the time available for air–fuel mixing, thus leading to important soot emissions increases, despite the lack of aromatics in the chemical structure of the fuel molecule.
- Finally, due to its higher cetane number, HVO shows a lower sensitivity towards changes in EGR rates and in SOI timings with respect to B5.

In conclusion, HVO showed an excellent adaptability to nowadays automotive diesel engines also as a neat fuel, without the necessity of a specific engine recalibration, allowing to achieve 3–4 % reduction in terms of $BSCO_2$ emissions, on a TTW basis, which coupled with an 81 % reduction on a WTT basis, could lead to an impressive 85 % reduction on a WTW basis.

While measured BTE variations were typically lower than 1 %, an increase in volumetric fuel consumption with HVO appears as unavoidable due to the lower density of the fuel, which cannot be fully compensated by its higher LHV. Nevertheless, the increase in volumetric fuel consumption with HVO was lower than 4 % in all the tested operating conditions, which could be regarded as acceptable from the final customer's point of view.

Finally, although soot emissions with HVO showed significant increases, likely due to the single injection strategy adopted for the study, impressive emissions reductions were observed for CO and HC (more than 40 and 50 %, respectively), with noticeable benefits also in terms of NOx (ranging from about −10 to −15 %).

CRediT authorship contribution statement

F. Millo: Writing – review & editing, Supervision, Project administration, Funding acquisition, Conceptualization. **M. Jafari:** Writing – original draft, Investigation, Formal analysis, Data curation. **A. Piano:** Writing – original draft, Supervision, Methodology, Investigation, Formal analysis, Conceptualization. **L. Postrioti:** Writing – original draft, Visualization, Methodology, Investigation, Data curation, Conceptualization. **G. Brizi:** Visualization, Validation, Software, Investigation, Data curation. **A. Vassallo:** Writing – review & editing, Validation, Supervision, Investigation, Conceptualization. **F. Pesce:** Writing – review & editing, Validation, Supervision, Resources, Conceptualization. **C. Fittavolini:** Writing – review & editing, Validation, Supervision, Project administration, Funding acquisition, Conceptualization.

Declaration of competing interest

The authors declare that they have no known competing financial interests or personal relationships that could have appeared to influence the work reported in this paper.

Data availability

The authors do not have permission to share data.

Acknowledgements

This work was supported by Eni S.p.A. through Politecnico di Torino – Eni Grant Agreement A37620.

Appendix A. Supplementary data

Supplementary data to this article can be found online at https://doi.org/10.1016/j.fuel.2024.132951.

References

[1] Regulation (EU) 2021/1119 of the European Parliament and of the Council of 30 June 2021 establishing the framework for achieving climate neutrality and amending Regulations (EC) No 401/2009 and (EU) 2018/1999 ('European Climate Law'), http://data.europa.eu/eli/reg/2021/1119/oj , accessed 09/07/2021.
[2] Ian Tiseo, "Carbon dioxide emissions from the transportation sector worldwide from 2000 to 2022, by sub sector", Statista, https://www.statista.com/statistics/1387814/carbon-dioxide-emissions-transport-subsector-worldwide/#statisticContainer , accessed 22/09/2023.
[3] Kramer U, Bothe D, Gatzen C, Pfannenschmidt, et al. "Future Fuels: FVV Fuels Study IVb- Final Report", FVV: How quickly can we be sustainable? (fvv-netde), accessed on Oct 2022.
[4] Krár M, Kovács S, Kalló D, Hancsók J. Fuel purpose hydrotreating of sunflower oil on CoMo/Al2O3 catalyst. Bioresour Technol 2010;101(23):9287–93. https://doi.org/10.1016/j.biortech.2010.06.107.
[5] Schwarz, L., Bargende, M., Dreyer, S., Baretzky, U. et al., "Methodical Selection of Sustainable Fuels for High Performance Racing Engines," SAE Technical Paper 2018-01-1749, 2018, doi: 10.4271/2018-01-1749.

[6] GSR, "GHG emissions from HVOlution produced by Eni Sustainable Mobility (ESM)," https://www.gsrtrasporti.com/wp-content/uploads/2023/11/Rivendicazione-emissioni-GHG-HVO_IQ-2023_Eng1_Rev.pdf, accessed Nov. 2023.
[7] Sonthalia A, Kumar N. Hydroprocessed vegetable oil as a fuel for transportation sector: A review. J Energy Inst 2019;92(1):1–17. https://doi.org/10.1016/j.joei.2017.10.008.
[8] Douvartzides SL, Charisiou ND, Papageridis KN, Goula MA. Green diesel: Biomass feedstocks, production technologies, catalytic research, fuel properties and performance in compression ignition internal combustion engines. Energies 2019;12(5). https://doi.org/10.3390/en12050809.
[9] Cheng Q, Tuomo H, Kaario O, Martti L. HVO, RME, and Diesel Fuel Combustion in an Optically Accessible Compression Ignition Engine. Energy Fuel 2019;33(3):2489–501. https://doi.org/10.1021/acs.energyfuels.8b03822.
[10] Cheng Q, Tuomo H, Kaario OT, Martti L. Spray dynamics of HVO and EN590 diesel fuels. Fuel 2019;245:198–211. https://doi.org/10.1016/j.fuel.2019.01.123.
[11] Zhang Z. Investigation Into Fuel Pre-treatments For Combustion Improvement On A Compression Ignition Engine. Newcastle: School of Engineering, Newcastle University; 2019. Ph.D. thesis.
[12] Bohl T, Smallbone A, Tian G, Roskilly AP. Particulate number and NOx trade-off comparisons between HVO and mineral diesel in HD applications. Fuel 2018;215:90–101. https://doi.org/10.1016/j.fuel.2017.11.023.
[13] Zhang, T., Andersson, M., Munch, K., and Denbratt, I., "Optical Diagnostics of Spray Characteristics and Soot Volume Fractions of n-Butanol, n-Octanol, Diesel, and Hydrotreated Vegetable Oil Blends in a Constant Volume Combustion Chamber," SAE Technical Paper 2019-01-0019, 2019, Doi: 10.4271/2019-01-0019.
[14] Dageförde T, Gröger K, Kawaharada N, Dinkelacker F. Velocity Field Measurements with High-Speed Structural Image Velocimetry in the Primary Atomization Region of Future Diesel Fuels. SAE Int J Adv & Curr Prac in Mobility 2021;3(1):378–86. https://doi.org/10.4271/2020-01-2112.
[15] Murtonen T, Aakko-Saksa P, Kuronen M, Mikkonen S, et al. Emissions with Heavy-duty Diesel Engines and Vehicles using FAME, HVO and GTL Fuels with and without DOC+POC Aftertreatment. SAE Int J Fuels Lubr 2010;2(2):147–66. https://doi.org/10.4271/2009-01-2693.
[16] Aatola H, Larmi M, Sarjovaara T, Mikkonen S. Hydrotreated Vegetable Oil (HVO) as a Renewable Diesel Fuel: Trade-off between NOx, Particulate Emission, and Fuel Consumption of a Heavy Duty Engine. SAE Int J Engines 2009;1(1):1251–62. https://doi.org/10.4271/2008-01-2500.
[17] Erkkilä, K., Nylund, N., Hulkkonen, T., Tilli, A. et al., "Emission performance of paraffinic HVO diesel fuel in heavy duty vehicles," SAE Technical Paper 2011-01-1966, 2011, doi: 10.4271/2011-01-1966.
[18] Omari A, Pischinger S, Bhardwaj O, Holderbaum B, et al. Improving Engine Efficiency and Emission Reduction Potential of HVO by Fuel-Specific Engine Calibration in Modern Passenger Car Diesel Applications. SAE Int. J. Fuels Lubr. 2017;10(3). https://doi.org/10.4271/2017-01-2295.
[19] Athanasios, D., Athanasios, D., Stylianos, D., Stella, B. et al., "Emissions Optimization Potential of a Diesel Engine Running on HVO: A Combined Experimental and Simulation Investigation," SAE Technical Paper 2019-24-0039, 2019, doi: 10.4271/2019-24-0039.
[20] Bhardwaj O, Kolbeck A, Kkoerfer T, Honkanen M. Potential of Hydrogenated Vegetable Oil (HVO) in Future High Efficiency Combustion System. SAE Int J Fuels Lubr 2013;6(1):157–69. https://doi.org/10.4271/2013-01-1677.
[21] Bortel I, Vávra J, Takáts M. Effect of HVO fuel mixtures on emissions and performance of a passenger car size diesel engine. Renew Energy 2019;140:680–91. https://doi.org/10.1016/j.renene.2019.03.067.
[22] Sugiyama K, Goto I, Kitano K, Mogi K, et al. Effects of Hydrotreated Vegetable Oil (HVO) as Renewable Diesel Fuel on Combustion and Exhaust Emissions in Diesel Engine. SAE Int J Fuels Lubr 2012;5(1):205–17. https://doi.org/10.4271/2011-01-1954.
[23] Hunicz J, Matijošius J, Rimkus A, Kilikevičius A, Kordos P, Mikulski M. Efficient hydrotreated vegetable oil combustion under partially premixed conditions with heavy exhaust gas recirculation. Fuel 2020;268. https://doi.org/10.1016/j.fuel.2020.117350.
[24] Postrioti L, Buitoni G, Pesce FC, Ciaravino C. Zeuch method-based injection rate analysis of a common-rail system operated with advanced injection strategies. Fuel 2014;128:188–98. https://doi.org/10.1016/j.fuel.2014.03.006.
[25] Postrioti L, Malaguti S, Bosi M, Buitoni G, Piccinini S, Bagli G. Experimental and numerical characterization of a direct solenoid actuation injector for Diesel engine applications. Fuel 2014;118:316–28. https://doi.org/10.1016/j.fuel.2013.11.001.
[26] Piano A, Millo F, Postrioti L, Biscontini G, et al. Numerical and Experimental Assessment of a Solenoid Common-Rail Injector Operation with Advanced Injection Strategies. SAE Int J Engines 2016;9(1):565–75. https://doi.org/10.4271/2016-01-0563.
[27] Piano A, Boccardo G, Millo F, Cavicchi A, et al. Experimental and Numerical Assessment of Multi-Event Injection Strategies in a Solenoid Common-Rail Injector. SAE Int J Engines 2017;10(4):2129–40. https://doi.org/10.4271/2017-24-0012.
[28] Postrioti L, Battistoni M, Ungaro C, Mariani A. Analysis of Diesel Spray Momentum Flux Spatial Distribution. SAE Int J Engines 2011;4(1):720–36. https://doi.org/10.4271/2011-01-0682.
[29] AVL, "Smoke Value Measurement with the Filter-Paper-Method, Application Notes, Copyright 2005 by AVL List GmbH, Graz - Austria, June 2005 AT1007E, Rev.".
[30] Boccardo G, Piano A, Zanelli A, Babbi M, Cambriglia L, Mosca S, et al. Development of a virtual methodology based on physical and data-driven models to optimize engine calibration. Transportation Engineering 2022;10. https://doi.org/10.1016/j.treng.2022.100143.
[31] Millo F, Debnath BK, Vlachos T, Ciaravino C, Postrioti L, Buitoni G. Effects of different biofuels blends on performance and emissions of an automotive diesel engine. Fuel 2015;159:614–27. https://doi.org/10.1016/j.fuel.2015.06.096.
[32] Hayashi J, Watanabe H, Kurose R, Akamatsu F. Effects of fuel droplet size on soot formation in spray flames formed in a laminar counterflow. Combust Flame 2011;158(12):2559–68. https://doi.org/10.1016/j.fuel.2015.06.096.
[33] García A, Monsalve-Serrano J, Villalta D, Lago Sari R, Gordillo Zavaleta V, Gaillard P. Potential of e-Fischer Tropsch diesel and oxymethyl-ether (OMEx) as fuels for the dual-mode dual-fuel concept. Appl Energy 2019;253. https://doi.org/10.1016/j.treng.2020.01.001.